Mapping available soil moisture content in an irrigated cotton growing field in the lower Gwydir valley

Melissa Head

Supervisor:

Dr John Triantafilis

Submited in fulfillment of the requirements for a Cotton, Communities and Catchments Cooperative Research Centre Project (Applied Geography)

School of Biological, Earth and Environmental Sciences,
Faculty of Science,
The University of New South Wales

July 2007

CONTENTS

1. INTRODUCTION

One of the key issues associated with sustainable irrigated agricultural production is maximizing water use efficiency. In order to achieve this there is a need to understand the water balance equation (i.e. Precipitation + Irrigation = Change in soil moisture + Deep Drainage + Runoff + Evapotranspiration). Whilst much research has focused on measuring evapotranspiration and deep drainage, little is known about the actual ability of various cotton growing soil types to store soil moisture. Different soil types are able to hold different amounts of water. Variation in soil types occurs not only on a regional and farm scale but also at the field scale. Because a field rarely contains a uniform soil type it is important to understand the spatial distribution of potential water storage to determine the optimal irrigation method and schedule to increase on-farm water use efficiency.

Qualitative soil moisture is measured in terms of field capacity (FC) and the permanent wilting point (PWP), representing the upper and lower limits of available water content. The ability of a soil to hold water is largely determined by soil texture and soil mineral. There is a general relationship between soil water characteristics and soil texture. Finer textured soils with greater contents of silt and clay tend to hold more water at field capacity than sandier soils, however as texture becomes finer the permanent wilting point does not increase at the same rate as field capacity. Therefore the volume percentage of soil water is not the same for all soil types. Clay content is therefore an important soil attribute to map because it largely determines the hydraulic properties and water holding capacity of a soil.

One of the main soil hydraulic properties is the moisture retention curve (MRC) as it expresses the relationship between field capacity and permanent wilting point of a soil. Measuring this directly at high spatial resolution is time consuming and costly. Consequently only a limited amount of data is actually collected. Traditional soil surveys do not adequately account for the spatial variability of various soil properties and there is a need to generate a large amount of data

from the limited amount of data collected. In this case, detailed soil information was obtained from soil cores obtained at calibration sites for the EM instruments. Ancillary data used included EM data and aerial photography. It was anticipated that this data could be interpolated out to the entire field.

Various models have been created to predict the MRC from the limited collected data such as particle-size distribution, soil bulk density etc. The prediction model used in this study was Neurotheta. Neurotheta uses neural networks to predict the MRC from known parametric pedotransfer functions such as the sand, silt and clay fractions.

Another consideration is the determination of suitable methods of spatial interpolation of the data collected. Several geostatistical techniques have been employed to predict the spatial distribution of clay content at the field scale using different combinations of ancillary data. These included kriging and multiple linear regression analysis.

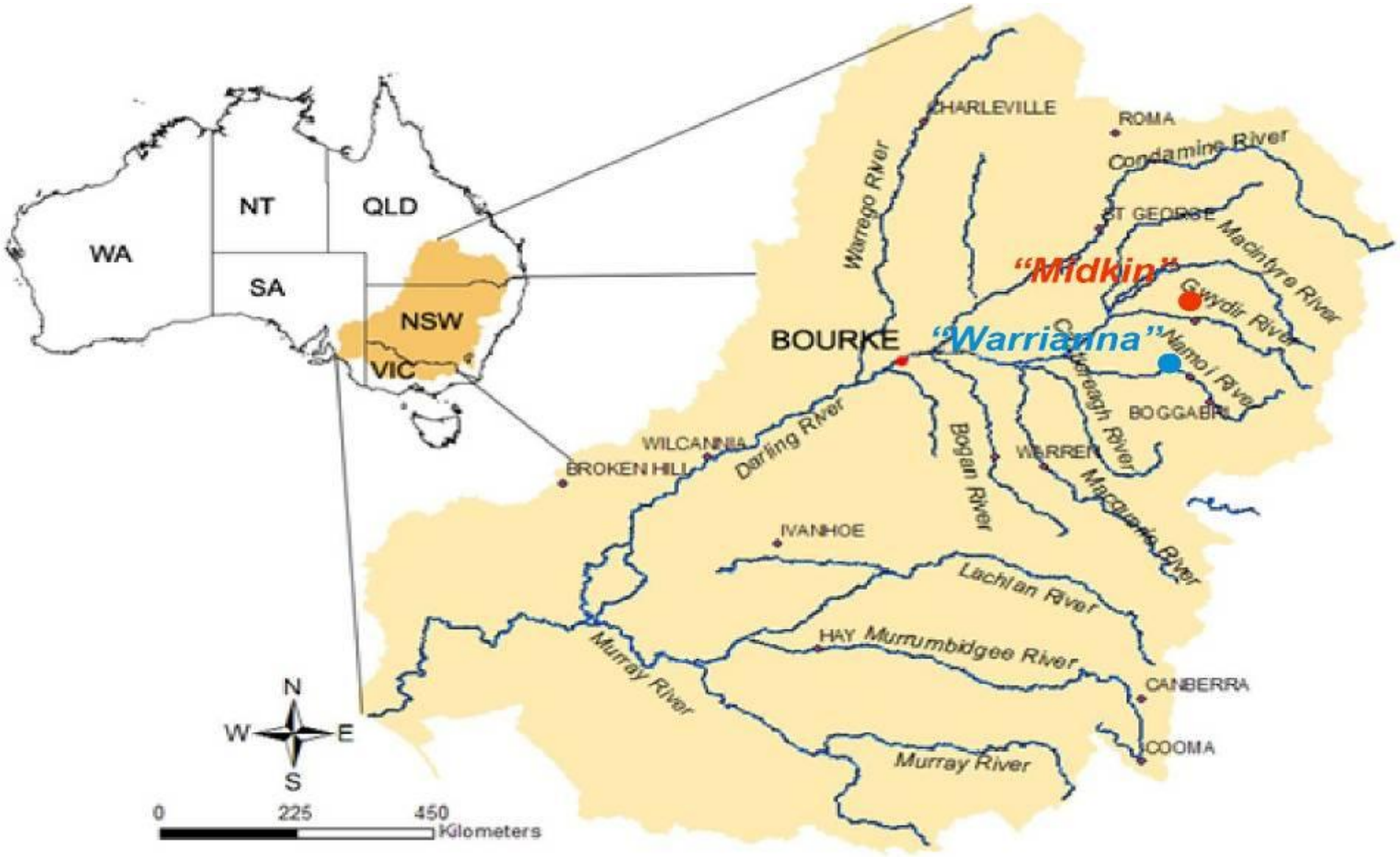

Figure 1 Study locations

2. MATERIALS AND METHODS

2.1 Study Areas

Auscott 'Midkin' is and irrigated cotton farm, which is predominately located in a large cotton growing district surrounding the township of Ashley in the lower Gwydir valley of northern New South Wales, Australia (Fig. 1). The field selected for this study, Field 11, covers approximately 244 ha (Fig. 2a). The field is dominated by self-mulching clays that have developed from alluvial deposits. The clay floodplains are the most widespread and are dissected in areas by watercourses. These watercourses leave behind old sand deposits on the landscape when the waterway changes course. The topography of the prior stream formations is slightly elevated and gently undulating. Within this field prior stream deposits are evident, which have various soil textures. The runs are approximately 1 km long except for the eastern end of the field where the shortest run is 100 m. The supply ditch is located on the southern margin of Field 11 and the field is irrigated in a northwesterly direction.

'Warrianna' Field 4 is located on the clay alluvial plains of the lower Namoi valley (Fig. 1), northwest of Wee Waa, New South Wales and supports cotton irrigation farming on self-mulching clays (Vertosols). It is located on a mixed farming enterprise which the clay alluvial plain is the dominant physiographic unit of the area and has a generally uniform topography except where current streams intersect. As shown in Figure 2b) 'Warrianna' Field 4 is approximately 800 m in the north-south dimension and 600 m in width. It therefore covers an approximate area of 80 ha. Irrigation is carried out by furrow irrigation with the head ditch located on the eastern side of the field. The water storage reservoir is located immediately to the west of this field with water pumped to head ditch via a supply channel which runs in parallel with the southern boundary of the field. In recent years, owing to problems with surface crusting caused by the application of sodic water, this field was deep ripped in order to bring to the surface naturally occurring gypsum and lime.

2.2 Ancillary Data

2.2.1 Electromagnetic Induction Instruments

Use of electromagnetic (EM) induction instruments is becoming increasingly popular because of its ability to collect ancillary data quickly and cheaply, and which can be used to infer spatially meaningful information about various soil properties. This includes, clay content, soil mineralogy, salinity and moisture. This is because EM instruments non-invasively measure bulk soil electrical conductivity (EC_a) by generating an alternating current through a transmitter coil at one end of the sensor. This induces a primary magnetic field to pass perpendicular to the coil orientation and into the soil. As this current passes through the soil, small eddy currents are created through any conductive material. The eddy currents then induce the creation of a secondary magnetic field. The strength of these eddy currents is a function of the amount of negative charge on clay particles, salinity levels, moisture, porosity and soil temperature. The receiver, on the other end of the sensor, detects the secondary magnetic field produced by the eddy currents in the soil. It also measures the primary magnetic field. The ratio of these two magnetic fields determines the apparent electrical conductivity of the soil. Two commercially available EM sensors that are commonly used in agricultural, soil and hydrological applications are the Geonics EM31 and EM38. The Geonics EM31 instrument has an intercoil spacing of 3.8 m and operates at a frequency of 6.4 kHz. It theoretically measures EC_a from a depth of 6.0m to 3.0 m in vertical and horizontal modes, respectively. It provides information mainly about the shallow vadose zone (i.e. depths beyond 1.5 m). The Geonics EM38 was developed to enable measurement of EC_a within the root-zone. It theoretically measures to 1.5 m and 0.75 m in the vertical and horizontal dipole modes, respectively. The two coils of the EM38 are spaced 1 m apart. The instrument operates at a frequency of 13.2 kHz.

Since the late 1970s electromagnetic (EM) induction techniques have been increasingly used to collect data at a high spatial resolution. EM response and measurements of ECa are primarily a function of soluble salts, clay content and mineralogy, soil water content and soil temperature

(Brevik and Fenton 2002). EM induction techniques in agriculture at the field scale were first applied to detect and delineate zones affected by salinity. Measurements of EC_a have also been used at the field scale as an indicator to infer a number of other soil properties such as: clay content and texture; soil water content; organic matter content. Relationships between EC_a measurements, soil properties and crop yield have also been inferred. Electromagnetic induction techniques were first proposed as an alternative to the four-electrode technique to aid salinity surveys (de Jong et al., 1979). They used an EM31 instrument and saw the main advantages of EM induction being its ability to sense continuously along a transect and therefore provide a rapid and easy method for detecting and mapping saline areas. Previous studies had used measurements of EC_a to map only salts or textural changes. Lesch et al. (1995) used EM induction data to predict field scale spatial salinity using multiple linear regression (MLR). It was compared to other geostatistics such as cokriging and found that MLR has its advantages over cokriging because it can use a smaller sample size but it is dependant on spatially uncorrelated results. The EM38 instrument has been used to estimate and map the deep drainage risk at the district level in northern New South Wales (Triantafilis et al. 2004). The EM survey was carried out in the Ashley (lower Gwydir valley) and Trangie (lower Macquarie valley) districts. Clay content and soil mineralogy are properties that greatly influence deep drainage and are properties that contribute to the bulk electrical conductivity measured by EM instruments. They found that low EC_a values were associated with sandy soils and higher values of EC_a were consistent with the plains of self-mulching clays similar to those of 'Midkin' Field 11 and 'Warrianna' Field 4. Low values of EC_a and coarser textured soils were found to be more susceptible to deep drainage. Conversely, higher ECa values characterised soil profiles where deep drainage was not high.

Sudduth et al. (2005) related EC_a with soil properties to describe within-field spatial variability. They found strongest correlations with clay content and CEC. They then used regressions to estimate clay and CEC as a function of EC_a with $r^2 \geq 0.55$. They surveyed twelve fields in six states (US). The implication of this work is that it may be feasible to develop

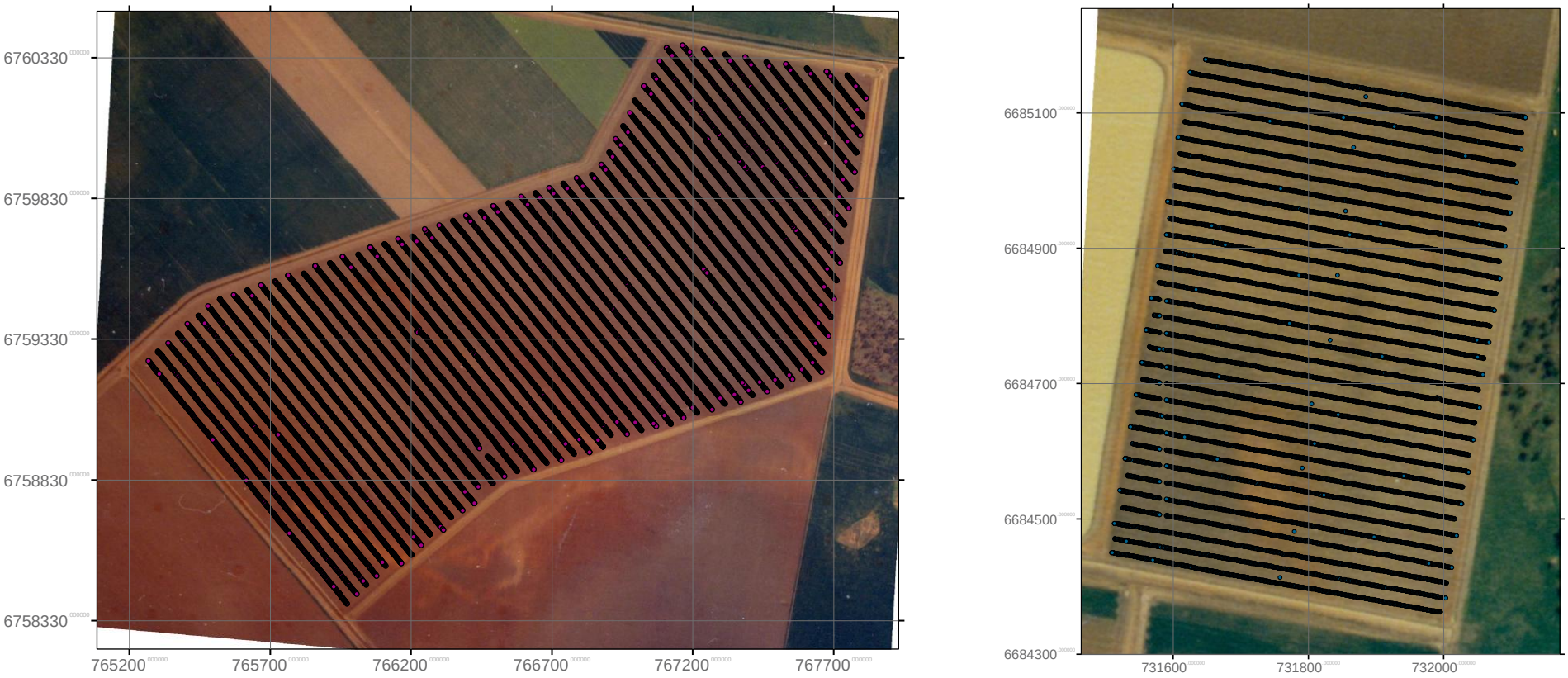

Figure 2 EM survey transect locations for a) ‘Midkin’ Field 11 and b) ‘Warrianna’ Field 4.

relationships between EC_a and clay and CEC that are applicable across a wide range of soil and climatic conditions.

Triantafilis and Lesch (2005) aimed to predict clay content south-east of Trangie in the Lower Macquarie Valley, New South Wales, Australia. The study was performed at a regional scale and used fuzzy k-means classification to classify the EM data into broad physiographic and hydrogeological units. Eight soil samples were taken from each of the five classes and analysed for clay content. In order to predict clay content across the study site hierarchical spatial regression model was developed using a composite signal variable and first order trend components. The resulting map generally reflected the surface clay content and provided information about the spatial distribution of subsurface clay variability.

2.2.2 Mobile EM Sensing Systems

In this study, data collected using a Mobile EM Sensing System (MESS) consisting of both EM31 and EM38 instruments attached to a lightweight tractor with PVC piping. A Global Positioning System (GPS) unit was used to georeference the EM signal data. The GPS assists in navigation by indicating to the operator where the current pass is and how to maintain the correct bearing. It also assists with locating and aligning the MESS for the next pass. The second GPS provides wide-area differential correction to ensure sub-metre accuracy.

Two separate MESS surveys are studied as part of this research. The EC_a data were obtained along 55 transects of 'Midkin' Field 11varying in length due to the shape of the field (Fig. 2a). Transects were approximately 48 m apart. EC_a data and GPS co-ordinates were recorded at approximately 1 m intervals along each transect. Due to the spatial nature of soil variability near the prior stream channel, a number of additional runs were traversed at intervals of 24 m between transects 17 and 24. EC_a measurements in 'Warrianna' Field 4 were carried out using the same method. A total of 32 passes were made with transects approximately 24 m apart (Fig. 2b).

MESS have been used a number of times previously to collect EM signal data rapidly, many of which have been conducted in the cotton irrigation regions of northern New South Wales. Triantafilis et al. (2001) used a MESS to determine the optimal spacing of transects for collecting EM data for spatial prediction was 24 m. They developed generalised additive models using various combinations of ancillary data and geostatistical methods of ordinary kriging, regression kriging and co-kriging and found that linear regression of average clay content and EC_a was most accurate. The study area used was also 'Midkin' Field 11.

Triantafilis et al (2202) used a MESS to assess cause and management of soil salinisation in an irrigated cotton field, located in the lower Namoi valley in northern New South Wales. The EM38 instrument was most strongly correlated with CEC which is related to variability of soil mineralogy, soil chemistry and soil texture. The correlation between EM31 and EM38 and the spatial distribution of EC_a provided a basis for determining the sampling strategy for the collection of data on selected soil properties which respond to the EM instruments. Because CEC was most strongly correlated with EC_a, this implied that soil mineralogy and salinity accounted for most of the response of the EM instruments. The EM signal data were interpolated onto a 5 m grid using Vesper (Minasny et al. 2005).

2.2.2 Aerial Photography

Soil colour can be related to soil type. Stannard and Kelly (1968) used aerial photography in concert with limited soil survey data to map soil type. Varvel et al. (1999) aimed to determine if relationships existed between spectral data in an aerial image and soil test results from an intensive grid soil sampling. They found correlations of visual data with soil properties demonstrated that a composite aerial image of bare soil provided information that could be used to direct sampling efforts and that other information such as knowledge of past management effects can affect these relationships. Bishop and McBratney (2001) also found that raw reflectance from aerial photos of the visible red, blue and green portion of the EM spectrum was a useful predictor variable that

exhibited high correlation with CEC. Digitised red, green and blue bands from aerial photographs of the study areas can therefore be potentially correlated with various surface soil types and soil texture. Raw reflectance red, green and blue values provide additional ancillary data which can be used in addition to the ground based EM data to develop regressions for statistical prediction.

The first step required in generating reflectance data requires the image to be digitised by scanning aerial photographs of both fields. This was done using a HP Scanjet 3770 digital flatbed scanner at a resolution of 1200 dpi. The images are then imported into ArcGIS and were georeferenced. Once the image was georeferenced it was opened in the program ERDAS Imagine. In this program the "extract by points" function was used to extract the red, green and blue pixel values onto each of the points of the 5 m grid. These values were then saved as a *txt file to allow manipulation in a spreadsheet or database.

Figure 3 shows the scanned colour aerial photographs of a) ‘Midkin’ Field 11, and b) ‘Warrianna’ Field 4. It is evident in Figure 3a) that the lighter and redder shades indictate the location and direction of a prior stream channel that cut across ‘Midkin’ Field 11. Interestingly the head ditch and supply channel are located along the southeastern end of Field 11, almost runs in parallel with the prior stream channel evident at the northern end of Field 12. The soil texture in these prior stream channels is generally silty clay. Conversely, the soil texture in the adjacent alluvial plain and as indicated by the grey hues to the north of the prior stream channel are medium to heavy clay.

Interestingly the head ditch which is located along the eastern margin of ‘Warrianna’ Field 4 is similarly characterised by coarser textured soil (i.e. silty clays). This is evidenced by the lighter red hues shown in Figure 3b). Progressively and to the west, the aerial photograph shows surface colour darken to brown grey shades apart from a red ellipse in the central and southern parts of Field 4.

Figure 3 Aerial photographs of a) ‘Midkin’ Field 11 and b) ‘Warrianna’ Field 4.

2.3 Soil Data

In 'Midkin' Field 11 soil sample sites were previously chosen by dividing the EC_a data collected from all transects into odd and even numbered transects. From each set, 23 sites of low, medium and high EC_a measurements were selected trying to spread soil sample sites as evenly across the field as possible (Fig. 4a). At each of the 46 sites an intact soil core was collected to a depth of 1.5 m and bulked into 0.3 m increments. The 5 samples collected at each of these sites were independently analysed using the pipette method (Coventry & Fett 1979) to determine particle-size fraction (PSF) or distribution (i.e. fine earth fraction or individual clay, silt and sand contents).

A similar approach was used to select 39 sampling locations across 'Warrianna' Field 4 (Fig. 4). The sites selected covered a range of high, intermediate and low values of EC_a and were spaced as evenly across the field as possible. An additional 9 sites were selected every four transects down the middle of the field running north to south. At each of the 39 sites an intact soil core to a depth of 2.1 m was collected and bulked into 0.3 m increments. Both sets of field samples were analysed for

a) soil moisture content (%);

b) pH of 1 part soil to 5 parts water;

c) electrical conductivity of a soil past extract (EC_e-dS m^{-1});

d) particle-size distribution using the hydrometer method and

e) effective cation exchange capacity (ECEC-mmol(+)/kg) (Tucker 1974).

Figure 4 Soil sample locations taken at a) ‘Midkin’ Field 11 and b) Warrianna ‘Field 4’

2.4 Calibration

2.4.1 Multiple Linear Regression

In environmental studies a regression relationship is often developed in order to make use of a more readily observable property (independent variable) which is strongly correlated with a variable of interest (dependent variable) but which is not so easily measured. So that the overall purpose of regression is to learn more about the relationship between one or several independent or predictor variables and a dependent or target variable. In the soil science literature the use of linear regression (*LR*) is well known. For example, Triantafilis et al., (2001) established a *LR* relationship between average soil clay content (target variable) and the more easily measured EM38-v signal data in an irrigated cotton field in the lower Gwydir valley. In this section a brief review is provided of this form of the predictor as well as multiple-linear regression (*MLR*).

Supposing that a target variable of interest, *z*, is determined at a limited number of locations *i*, *i* = 1....*n*, and $\boldsymbol{X}$ being a *p* x *n* matrix of *p* predictor variables observed at the same locations. The *LR* model relating $\boldsymbol{z}$ with $\boldsymbol{X}$ is written in matrix form:

$$\boldsymbol{z} = a + \boldsymbol{X}b + \varepsilon$$

where *a* and *b* are constants, and ε the error term with zero mean and constant variance. The regression coefficient, *b*, is not known *a priori*, but could be estimated by ordinary least-squares methods. The interest focuses on how model (5.1) can be used to predict $\boldsymbol{z}$ at location s_0 where only x_r (row of predictor variables) has been determined.

In the multivariate case, when there is more than one independent variable, the regression line cannot be visualized in the two dimensional space, but can be computed just as easily. For example, if in addition to having EM38-v signal data Triantafilis et al. (2001) had additional predictors of clay content available (e.g., EM31-v) a *MLR* equation containing all predictor variables could be constructed. In general then, *MLR* procedures will estimate a linear equation of the form:

$$\boldsymbol{z} = a + \boldsymbol{X_1}b_1 + \boldsymbol{X_2}b_2 + ... + \boldsymbol{X_2}b_{2+} \varepsilon \qquad (2)$$

It should be noted that in this equation, the regression coefficients (or *b* coefficients) represent the independent contributions of each independent variable to the prediction of the dependent variable. Another way to express this fact is to say that, for example, variable X_1 is correlated with the ***z*** variable, after controlling for all other independent variables.

2.4.2 Ordinary Kriging

Ordinary kriging (*OK*) is one of the most basic of kriging methods. It provides an estimate at an unobserved location of a variable ***z*** based on the weighted average of adjacent observed sites within a given area. The theory is derived from that of regionalized variables (Matheron, 1971) and can be described by considering an intrinsic random function denoted by $Z(s_i)$, where s_i represents all sample locations, i=1,...,n. An estimate at unsampled locations is the weighted average given by the *OK* predictor:

$$z^*(s_o) = \sum_{i=1}^{n} \lambda_i z(s_i) \qquad (3)$$

where, λ_i are the weights assigned to each of the observed sample sites. These weights sum to unity so that the predictor provides an unbiased estimation.

$$\sum_{j=1}^{n} \lambda_i = 1 \qquad (4)$$

Conventionally, a semi-variogram is inferred and modeled for the entire data set, and therefore summarises and is used to describe the spatial covariance structure of the area. The weights are calculated from the matrix equation

$$c = A^{-1}b \qquad (5)$$

where A is a matrix of semivariances between the data points; b is a vector of estimated semivariances between the data points and the points at which we wish to predict the variable z; and c is the resulting weights and the lagrange multipliers ψ. The prediction variance is also estimated at each unknown location using

$$\sigma^2(x_o) = \psi + \sum_{j=1}^{n} \lambda_i \gamma(x_i, x_o) \quad (6)$$

where ψ is a Lagrange multiplier and $\gamma(x_i,x_o)$ the semi-variogram model

Another approach is to estimate *z* at unsampled locations by modeling the variogram in the neighbourhood. Haas (1990a; 1990b) developed this approach to map variables affected by spatial trend or changing covariance structure. The method enables a local spatial variance model to be developed around each unknown point as in equations 3-5. The Vesper software package (Minasny *et al.,* 1999) was used to generate local variograms and to interpolate data.

The EM31 and EM38 data for both the 'Midkin' Field 11 and 'Warrianna' Field 4 surveys was kriged onto a common 5m grid using ordinary kriging. The MLR equations developed between EM signal data and RGB bands to estimate PSF were then used to estimate PSF at each 5 m grid node.

2.5 Estimating Available Water Content

2.5.1 Soil Moisture Potential

Most of the issues about soil water relate to its movement. An indication of the tendency of soil water to move is expressed by soil water potential. Classical physics recognises kinetic (movement) and potential (position) energy. In soil, water does not move rapidly so kinetic energy is negligible. Therefore, water moves constantly in the direction of potential energy (i.e. wet to dry soil), where gradient of potential energy with distance is moving force causing flow. There are three important factors affecting soil water energy level. The first force is gravity, where energy level of water at a certain height is always higher than water at lower levels; hence difference causes downward flow.

The Gravitational Potential (ψ_g) of soil water is assessed by gravity times height of water above some reference elevation. Secondly, forces of attraction between water and ions and other solutes result in osmotic forces that reduce water energy state. Low Osmotic Potential (ψ_m) results

from high solute (e.g. salts) concentrations which make it difficult for plants to remove soil water even though it may be present. Finally, adhesion (attraction) of water to soil matrix, provides a matric force (i.e. adsorption and capillarity) which reduces energy of water particles near surfaces. These forces and pressures are significant in specific field situations, however matric potential (ψ_m) is important in all unsaturated soil because the interactions between soil and water are ubiquitous. The movement and availability of water is primarily determined by ψ_m.

2.5.2 Soil Moisture Characteristic

Figure 5 shows the Soil Moisture Characteristic and who it relates Soil Wetness (w or θ) to the ψ_m can be used to ascertain the Available Water Content (AWC) and can be used to help irrigators and farmers determine soil water status in soil after rainfall and irrigation events. The shape of the curve is related to various physical and chemical soil properties such as texture, which are unique for each soil. The soil moisture characteristic contains other soil information such as Saturation Point, Field Capacity and Permanent Wilting Point. A soil becomes saturated after an irrigation event or for short periods of time during heavy rain. At this point soil is said to be at its Maximum Retentive Capacity and the ψ_m is close to zero (i.e. ~ 0).

Water in the macropores drain under the forces of gravity and after a couple of days soil is said to be at Field Capacity (FC). Field Capacity refers to the point where soil holds the most water that can be used by plants with sufficient air filled pore space (i.e. >10%) for plant growth and other aerobic activity. It corresponds to θ at about –10 to –33 J/kg ψ_m. Water in excess of FC drains too quickly for plant use.

Permanent Wilting Point (PWP) describes the lower limit of plant available water. It refers to the point where the only remaining soil water is held in the soil's micropores. Water molecules are bound tightly by adhesive forces to individual soil particles in thin films approximately 10 molecules thick and plants are generally unable to generate water potentials low enough to remove the water from the soil. At this stage θ is at *P.W.P.* and by convention is taken to be amount of

water retained by soil when the ψ_m is –1,500 J/kg. The amount of water held between FC and PWP is termed the Available Water Content and is a measure of the amount of water in the soil that is "potentially" available to plants.

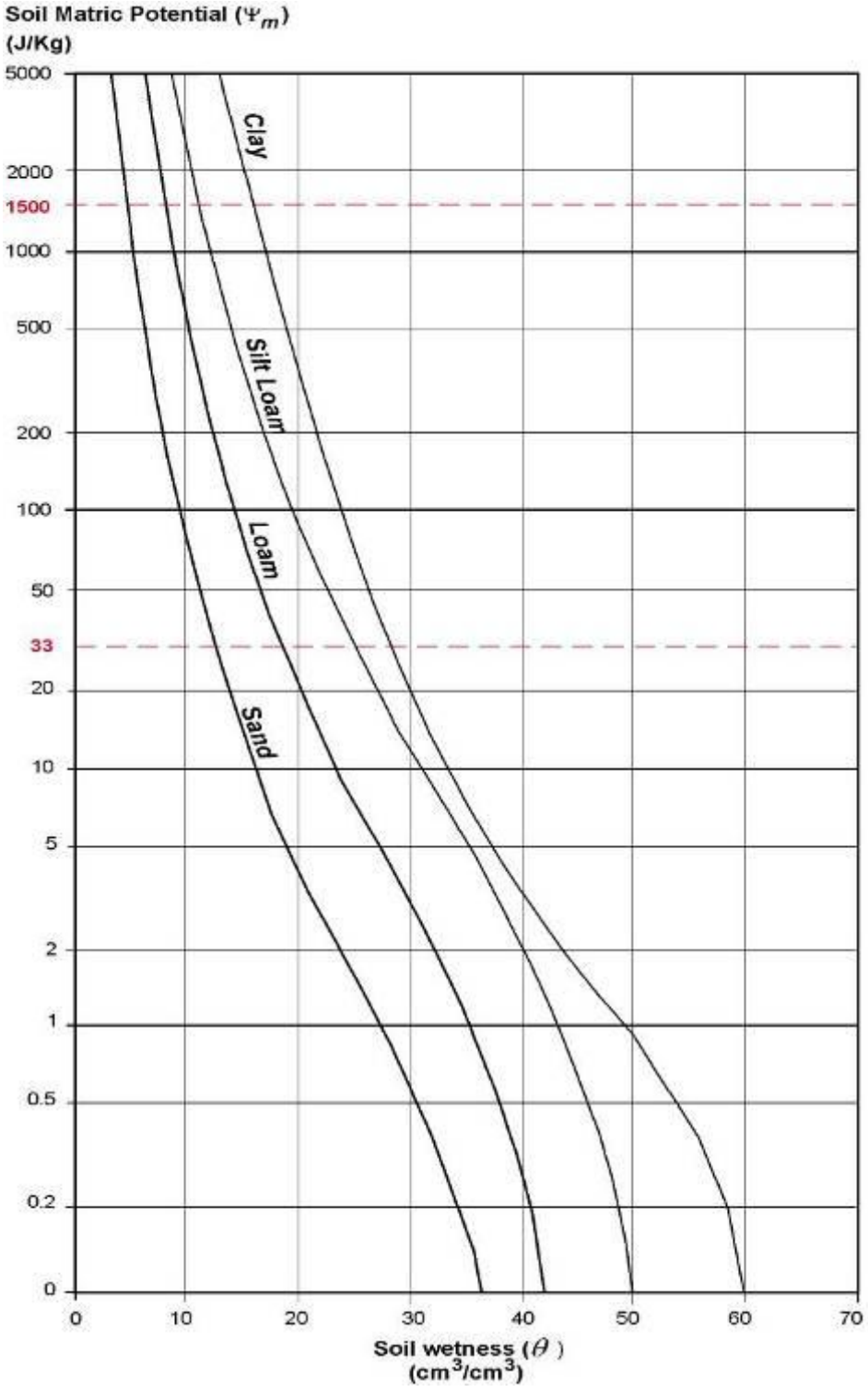

Figure 5 Relationship of soil texture to soil wetness and soil matric potential

2.5.3 Soil Texture and Soil Water Classification

Soil texture is strongly related to a soil's water holding capacity. Soil texture is a function of its composite fractions of clay, silt and sand. For soils with greater contents of silt and clay (i.e. finer textures), the amount of water held at FC tends to be greater than for coarser textured soils. The water held at potentials below the wilting coefficient (unavailable to plants) also increases with finer soil texture, but not as sharply. Therefore, the amount of water held at potentials between those of FC and PWP tends to be greatest in medium-textured soils such as silt loams. As clay content increases higher clay content soil increase more sharply at PWP than at FC. Medium-textured soil known as loams, have properties in between those of coarse and fine textures. Silty loams to sandy-clay loams have a good capacity to retain water without becoming waterlogged. Fine-textured soils range from silty clay to heavy clay. They have a large total pore space but these are mostly micropores. Therefore these soils can hold a lot of water but are poorly aerated and often waterlogged.

Figure 5 shows the soil moisture curves of various soil textures.

Figure 6 shows the relationship of soil texture to the available water content. From the data prsented it can be seen that sand holds the least amount of water at field capacity and permanent wilting point. As such sandy soil has a total available water content of approximately 0.4 mm/cm. A clay textured soil can hold the most amount of water at field capacity (approximately 3.2 mm/cm) and permanent wilting point (approximately 2.0 mm/cm) however this means the total available water capacity is only 1.2 mm/cm. A silty loam reaches field capacity when moisture is approximately 2.9 mm/cm and has a volumetric moisture of 1.0 mm/cm at permanent wilting point. In contrast to the clay textured soil, the total available water content for this texture class is 1.9 mm/cm.

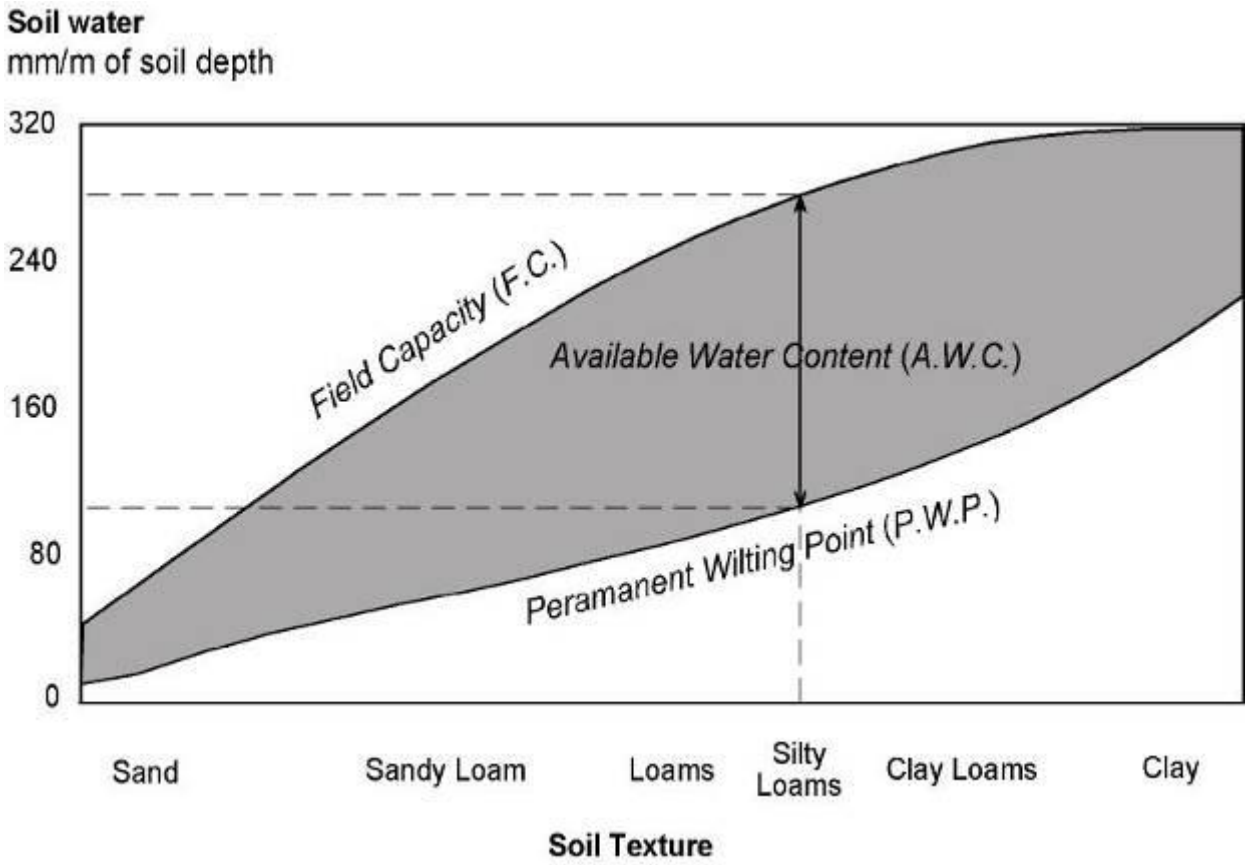

Figure 6 Relationship of soil texture to available water content (after Foth, 1990)

2.5.4 Pedotransfer Functions and Neurotheta

While the MRC provides valuable information about the available water content it is not a readily available soil property. The soil moisture retention curve of a soil sample is a time-consuming to measure directly. Pedotransfer Functions is a term increasingly finding its way into the literature. It can be defined as a predictive function of certain soil properties which are expensive to measure but which can be estimated using other available or easily measured properties. This commonly includes measurements of field morphology, soil texture, structure and pH. Pedotransfer functions add value to this basic information by translating them into estimates of other more laborious and expensively determined soil properties, such as the Soil Moisture Characteristic, specifically field capacity, permanent wilting point and available water capacity. Pedotransfer functions utilize various regression analysis and data mining techniques to extract rules associating basic soil properties with more difficult to measure properties.

Neural network theory is used to refer to a branch of computational science that uses neural networks as models to either simulate or analyse complex phenomena. The model used in this study to predict the available water content was Neurotheta. Neurotheta uses a calibrated neural network to predict parameters of the van Genuchten function to describe the relationships between water content and pressure head and hydraulic conductivity, from soil particle size distributions from basic soil properties of Australian soil (Minasny & McBratney 2002).

Minasny & McBratney (2002) proposed a new objective function to train neural networks for deriving the parameters of a soil hydraulic model. Conventionally parametric PTFs train the network to fit the estimated van Genuchten parameters. The aim was to predict water retention by training the network to fit the measured water content. The new objective function for neural network training predicts the van Genuchten parameters and minimises the difference between the measured water content and the one calculated from the predicted parameters. The usual steps for neural network training involve 1) fitting the van Genuchten equation and estimating the parameters then 2) training the neural network to predict the parameter vector from basic soil properties by minimising the objective function. They termed this the *neuro-p* method; a neural network with an objective function that matches the parameters. The *neuro-m* method continues with further fine-tuning steps by 3) using the trained weights as an initial guess for the second training, which fine tunes the estimates, then 4) for each soil sample, predicting the hydraulic parameters with the trained weights, and calculating water content using the van Genuchten equation at each of the measured potentials, then 5) adjusting the weights to minimise the difference between the predicted and measured water content with the optimisation routine.

The new method was compared to the performance of different PTFs trained using different objective functions. They found that using Australian soil hydraulic data as a training set, *neuro-m* predicted the water retention from bulk density and particle-size distribution with a mean accuracy of $0.04 m^3 m^{-3}$. The relative improvement of *neuro-m* over *neuro-p* was 13%.

3. RESULTS AND DISCUSSION

3.1 Basic Summary Statistics

Table 1 shows the basic summary statistics pertaining to the 27646 and 31520 EM31 and EM38 signal data readings made across 'Midkin' Field 11 and 'Warrianna' Field 4, respectively. Table 1, Part 1 shows the EM31 and EM38 statistics for 'Midkin' Field 11. The EM38 data has a minimum of 28 mS/m and a maximum of 212 mS/m and is slightly left-skewed and leptokurtic. The mean and median are similar meaning that the data is normally distributed. The EM31 signal readings did not cover as great a range as the EM38 with a minimum of 65 mS/m and a maximum of 220 mS/m. The data is similarly left-skewed and leptokurtic. The EM38 data is also normally distributed with a mean of 110 mS/m and a median of 111 mS/m. The positive kurtosis of both signal data sets can be attributed to the readings taken over a prior stream channel. Part 2 of Table 1 shows the equivalent statistics for 'Warrianna' Field 4. The EM38 signal data ranges from 50-184 mS/m and the EM31 data ranges from 75-234 mS/m. The mean EM31 reading is 141 mS/m compared to the mean EM38 reading of 110 mS/m. Both means are are also very similar to the medians and so can be considered to be normally distributed. In contrast to the 'Mikin' Field 11 signal data, both the EM38 and EM31 signal data for 'Warrianna' Field 4 is slightly right-skewed and platykurtic. Overall the EM31 readings had the highest mean for both 'Midkin' Field 11 and 'Warrianna' Field 4.

Table 1 Basic summary statistics of EM signal data

1) 'Midkin' Field 11							
EM Signal Data *N*=27646	Mean	Median	SD	Min	Max	Kurtosis	Skewness
EM38	134.39	135.85	18.30	28.09	211.87	3.13	-1.00
EM31	170.01	170.65	16.86	64.66	219.98	3.45	-0.96
2) 'Warrianna' Field 4							
EM Signal Data *N*=31520	Mean	Median	SD	Min	Max	Kurtosis	Skewness
EM38	110.35	110.92	21.91	50.00	184.00	-0.95	0.02
EM31	141.36	139.00	30.19	75.00	234.20	-0.99	0.12

Part 1 of Table 2 shows the basic summary statistics of the particle-size analysis of the soil samples taken from ‘Midkin’ Field 11 and ‘Warrianna’ Field 4. Clay represented the dominant particle-size fraction in ‘Midkin’ Field 11 with a mean of 53%. The distribution of clay was normally distributed and is leptokurtic and left-skewed. Silt content ranges from 19 to 38 and has a mean and median of 29. This distribution has a negative kurtosis (i.e. platykurtic) and is also left-skewed. The distribution of sand-size particles had the greatest range of 53 with a mean sand content of 17%. The data is strongly leptokurtic and right-skewed. The skew can be explained by the prior stream channel which has a much higher sand content than the rest of Field 11 is not representative of the mean level of sand content of the rest of the field. Part 2 of Table 2 shows the summary statistics of the particle-size distributions of ‘Warrianna’ Field 4. Clay-sized particles had the highest mean of 53% with the greatest range with a minimum of 32% and a maximum of 64%. The distribution is platykurtic and left-skewed. The mean silt content of Field 4 was 22% and ranged from 10% to 29%. The distribution was leptokurtic and right-skewed slightly. Sand content was normally distributed and had a mean and median of 18%. The range was 7% to 37% and the data was leptokurtic and right-skewed also.

Table 2 Summary statistics of average particle-size distributions from soil sample locations

1) 'Midkin' Field 11							
N=81	Mean	Median	SD	Min	Max	Kurtosis	Skewness
Average Clay	53	54	10	21	69	0.20	-0.70
Average Silt	29	29	12	19	38	-0.16	-0.22
Average Sand	17	13	11	7	60	5.62	2.17
2) 'Warrianna' Field 4							
N=39	Mean	Median	SD	Min	Max	Kurtosis	Skewness
Average Clay	52	54	8	32	64	0.52	-0.77
Average Silt	22	29	5	10	29	0.48	0.19
Average Sand	18	18	7	7	37	1.38	0.90

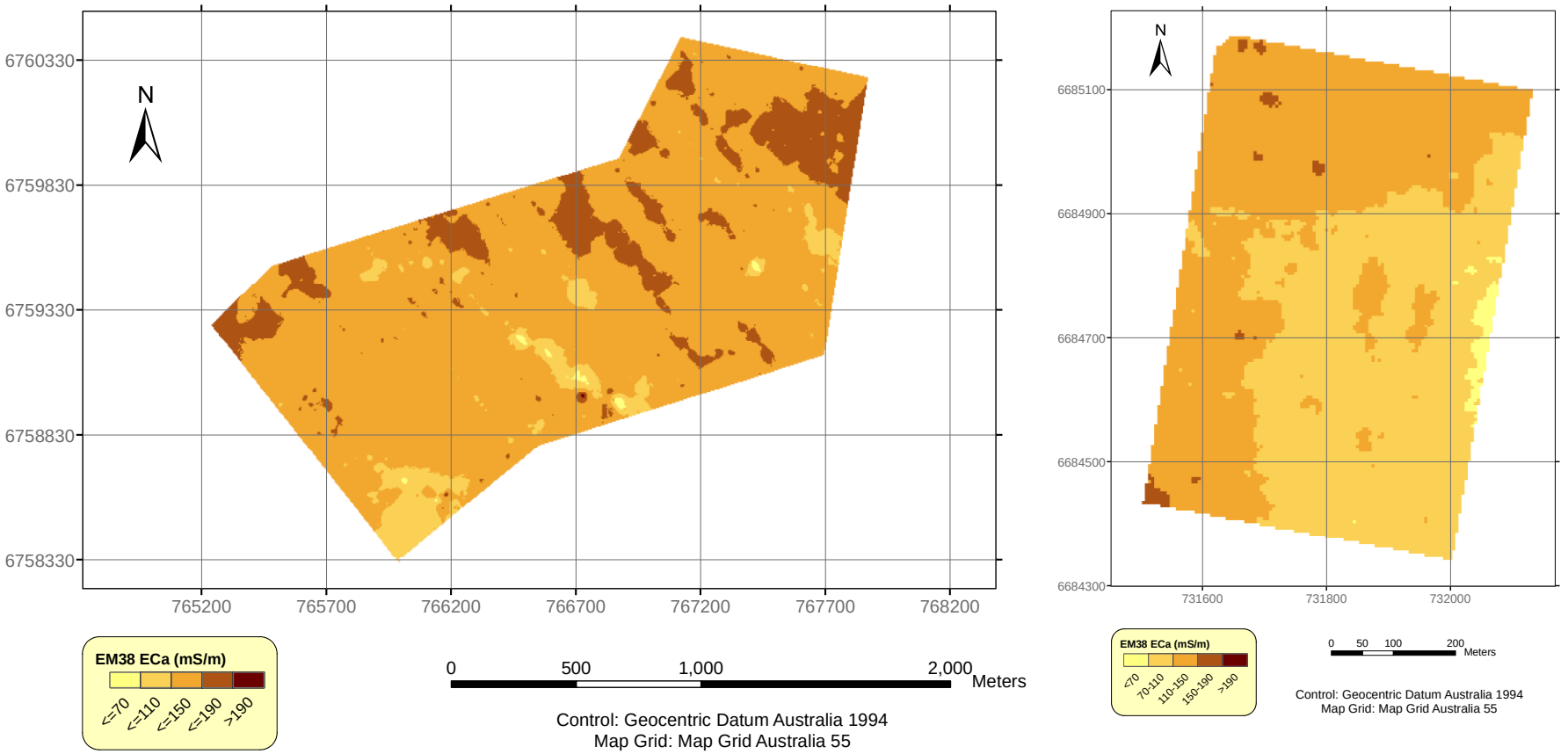

Figure 6 Spatial distribution of interpolated EM38 signal data across a) 'Midkin' Field 11 and b) 'Warrianna' Field 4.

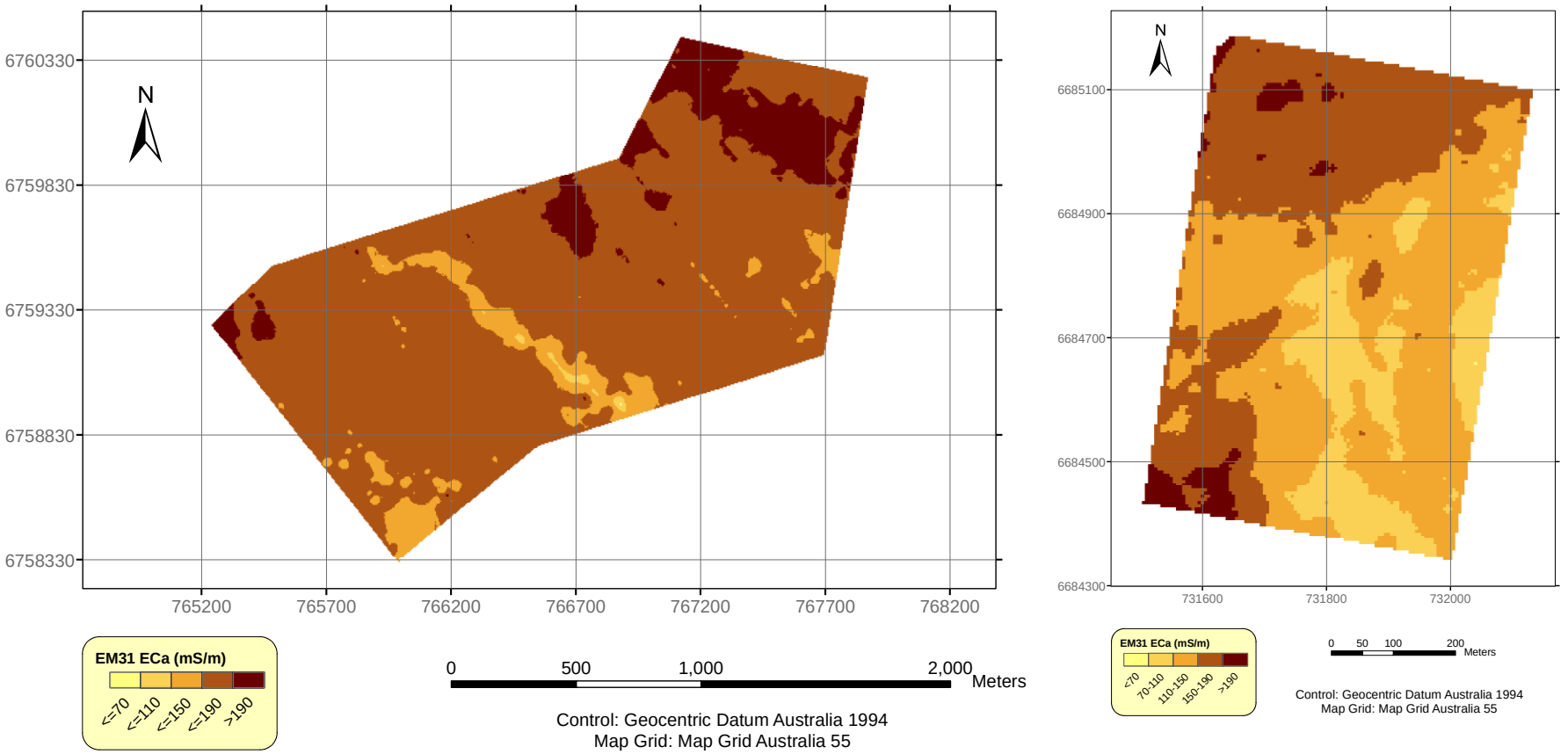

Figure 7 Spatial distribution of interpolated EM31 signal data across a) 'Midkin' Field 11 and b) 'Warrianna' Field 4.

3.2 Spatial distribution of ancillary data

3.2.1 Electomagnetic (EM38 and EM31) Signal Data

Figure 6a) and b) show the spatial distribution of EM38 signal data interpolated from the EM transects using OK onto a 5 m grid across 'Midkin' Field 11 and 'Warrianna' Field 4, respectively. The dark brown shaded areas indicate where EM38 signal data is highest (i.e. > 190 mS/m). Conversely, the yellow shaded areas indicate where EM38 signal data is lowest (i.e. < 70 mS/m). As mentioned previously the EM38 measures bulk electrical conductivity to a depth of approximately 1.5 m. The EM38 survey measured higher overall bulk electrical conductivity in 'Midkin' Field 11 than in 'Warrianna' Field 4 where the mean ECa of the 'Midkin' EM38 survey was 134 mS/m and the mean ECa of 'Warrianna' was 110 mS/m (Table 1).

The northeastern corner of the 'Midkin' Field 11 (Fig. 5a) includes the largest area of the highest EC_a. Other patches of high EC_a occur along the northern boundary. These areas of higher EM38 signal data readings coincide with where soil colour (as indicated in aerial photograph) is grey and where soil texture is clayey. The areas of low EM38 signal data readings coincide with the location of the prior stream channels. Sand particles lack the negative charge of clay particles and therefore are less conductive. Figure 6b) shows the highest ECa in 'Warrianna' Field 4 occurs generally on the northern and western margin (i.e. 110-150 mS/m). The reason for this is that the soil texture is silty. The rest of the field is dominated by levels of ECa from 70-100 mS/m. These lower EM38 signal readings are consistent with the siltier textures which characterised this part of 'Warrianna' Field 4.

Figure 7a) and b) show the spatial distribution of the interpolated EM31 signal data across 'Midkin' Field 11 and 'Warrianna' Field 4, respectively. As mentioned previously, the EM31 instrument measures bulk electrical conductivity (EC_a) to a depth of approximately 6.0m in the vertical position. The mean ECa was again higher for 'Midkin' Field 11 (i.e. 170 mS/m) than it was for 'Warrianna' Field 4 (i.e. 141 mS/m) (Table 1).

In Figure 7a) the prior stream channel running through the middle of 'Midkin' Field 11 can be seen more clearly from differences in EC_a than can be discerned in the EM38 survey, however, the EC_a is more uniform along the northern boundary compared to Figure 6a). Compared to the Figure 6b), Figure 7b) shows more spatial variation in ECa for of 'Warrianna' Field 4. The eastern section of the field is dominated by two levels of EC_a (i.e. 70-100 mS/m and 110-150 mS/m).

Overall the EM31 survey data for both 'Midkin' Field 11 and 'Warrianna' Field 4 has higher bulk electrical conductivity than the EM38 survey for both fields, but both represent similar spatial variability of EC_a across both fields. The stream channels are evident in both surveys but are best represented in the map of EM31 signal data. The main palaeochannel is most accurately mapped by the EM31 because the EM31 is operating to a greater depth where the sandier textures occur. This sandy layer is overlain by the alluvial silty clay textured soil which dominates the field. Both EM31 and EM38 surveys indicate that 'Warrianna' Field 4 is mostly dominated by the lower EC_a values occurring in the eastern and southeastern parts of the field. The areas of highest electrical conductivity occur in the northwestern and southwestern corners of the field. These patterns in EC_a are apparent in both surveys.

3.2.2 Spatial Distribution of Red, Green and Blue Spectral Bands

Figure 8 shows the spatial distribution of red band reflectance as extracted from the digitised aerial photos shown in Figure 2. Figure 8a) shows the spatial distribution of the red band across 'Midkin' Field 11. It is evident that the more intense reflectance values in the red band (i.e. >200) are consistent with the location of the prior stream channels that run through the central part of Field 11 and also in the southwest corner. Here the soil is generally coarser textured (i.e. sandier) in nature. These sand grains are covered or tinted if you will by iron oxides which are actually visibly red at the surface level. Figure 8b) shows the distribution of red band reflectance extracted from the aerial photo of 'Warrianna' Field 4. The higher reflectance values (i.e. >160) are consistent with the locations of the sandier parts of the field which are also visible in the aerial photograph.

The small elliptical shape in the southern part of the field and the eastern border are lighter in colour than the rest of the field. Here, the 'redder' parts of Figure 8b) are also associated with siltier textured soil with the individual particles again coated with iron oxides which contribute to the high reflectance of visible red. Overall, 'Warrianna' Field 4 has lower red reflectance than that observed in the aerial photograph of 'Midkin' Field 4.

Figure 9a) shows the spatial distribution of green reflectance values extracted from the aerial photograph of 'Midkin' Field 11. The highest green reflectance values (i.e. >120) occur mostly in the eastern sections of the field and along the northern boundary. It grades into lower reflectance values towards the southwestern and southern parts of the field. The palaeochannels are also evident in Figure 9a) and can be noted clearly because of their high reflectance values, although interestingly the southern end of the palaeochannel in the middle of the field has high reflectance values whereas at the northern end the reflectance is low. Figure 9b) shows the spatial distribution of the green reflectance of 'Warrianna' Field 4. The highest values occur along the eastern boundary and along approximately E6684900. These locations coincide roughly with the areas of high reflectance in Figure 8b). This can be related to the sandier textures known to exist within these parts of the field.

Figure 10a) shows the spatial distribution of blue reflectance of 'Midkin' Field 11. The prior stream channels are not discernable in this figure. The highest values are again, occurring in the eastern end of the field and grading into lower values towards the western and southern ends of the field. This is the only notable trend. Figure 10b) shows the spatial distribution of blue reflectance values across 'Warrianna' Field 4. This figure does not yield much useful information. Blue reflectance values are almost uniform across the field except for eastern parts of the field where slightly higher values occur.

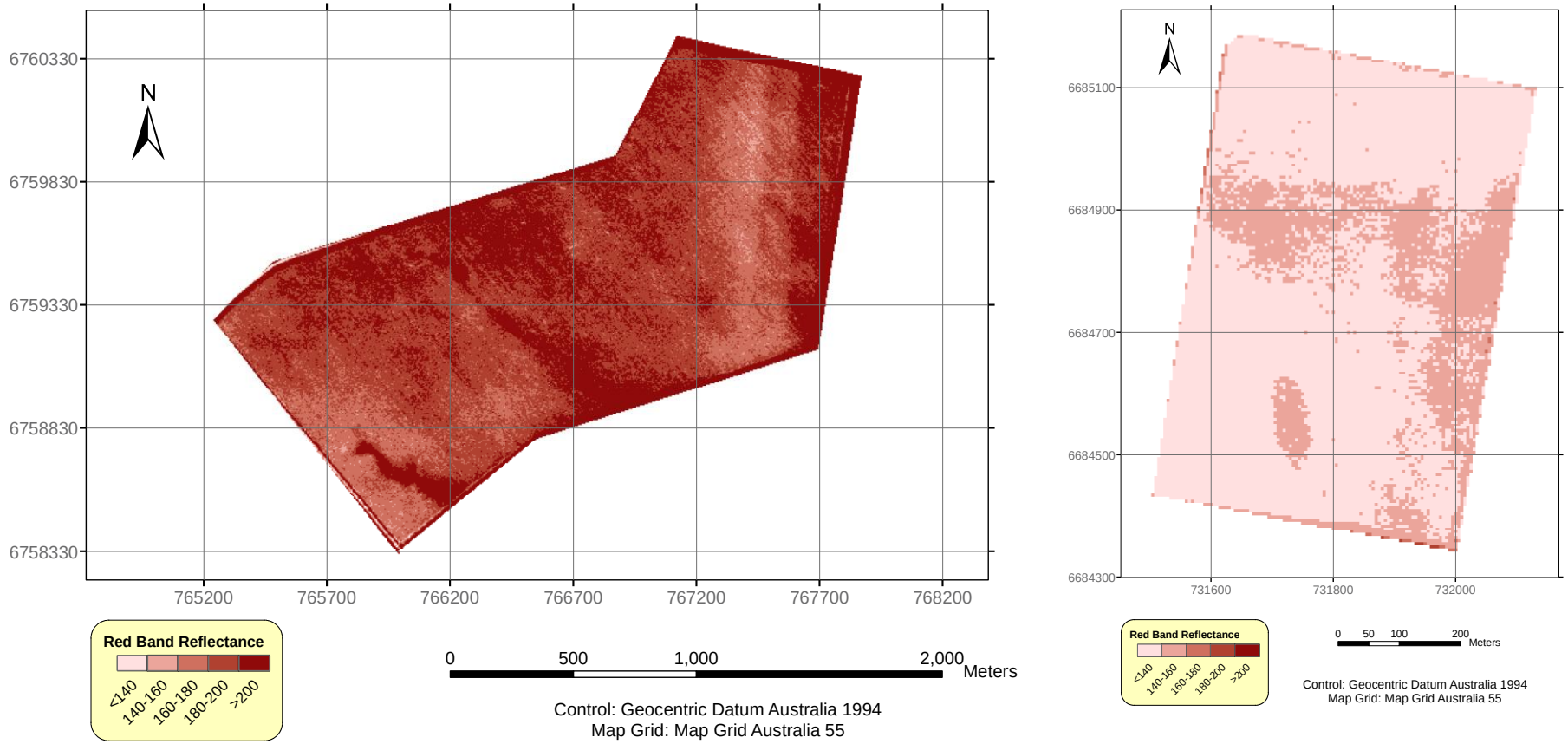

Figure 8 Spatial distribution of red band across a) 'Midkin' Field 11 and b) 'Warrianna' Field 4.

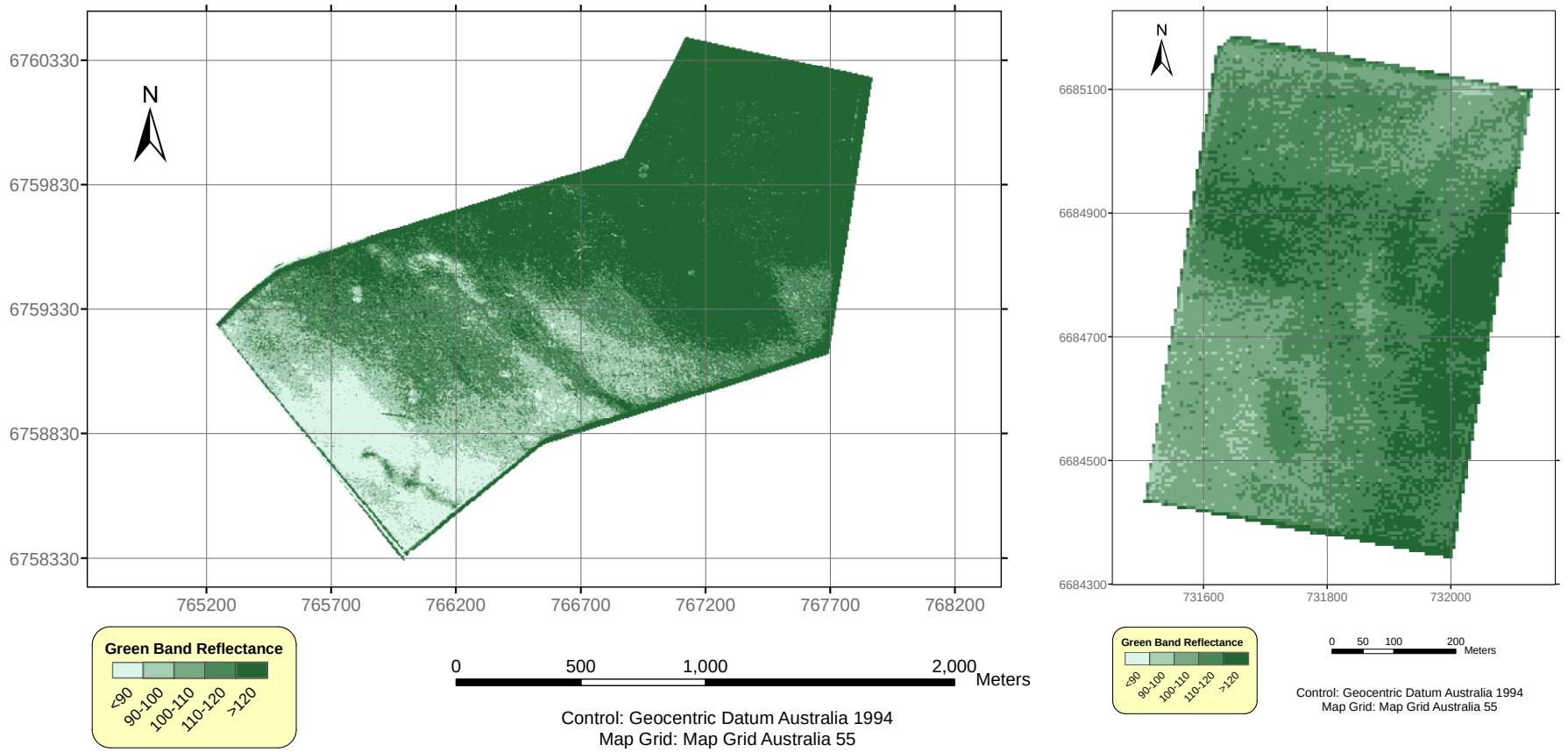

Figure 9 Spatial distribution of green band across a) 'Midkin' Field 11 and b) 'Warrianna' Field 4.

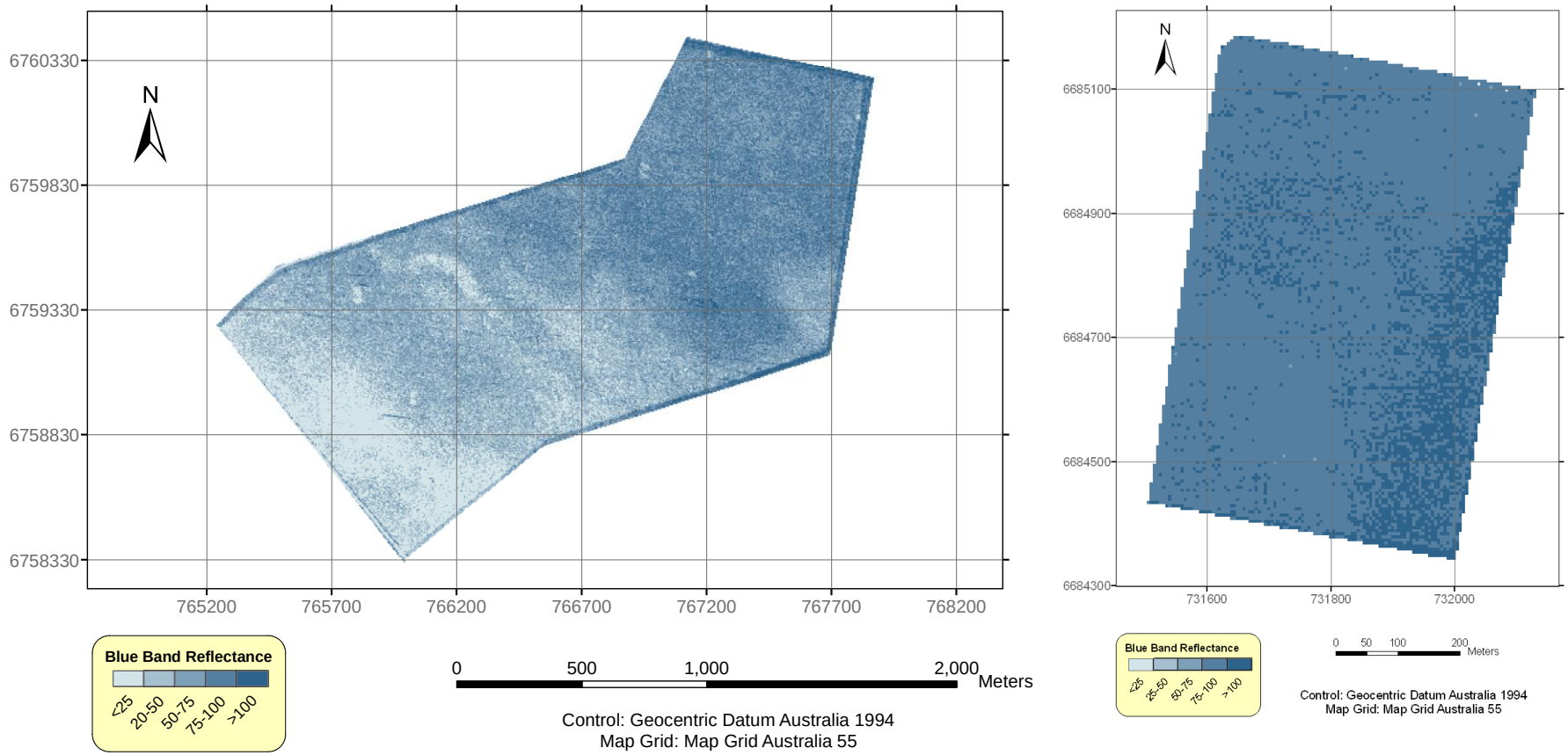

Figure 10 Spatial distribution of blue band across a) 'Midkin' Field 11 and b) 'Warrianna' Field 4.

3.3 MLR Analysis

Predictive models were developed by stepwise MLR from the ancillary information collected from the 81 sample locations for ‘Midkin’ Field 11 and the 39 sample locations for ‘Warrianna’ Field 4. Stepwise regression refers to regression models in which the choice of predictive variables is carried out by an automatic procedure. The main approaches are: a) forward selection, which involves starting with no variables in the model, trying out the variables one by one and including them if they are 'statistically significant'; b) backward selection, which involves starting with all candidate variables and testing them one by one for statistical significance, deleting any that are not significant or c) methods that are a combination of the above, testing at each stage for variables to be included or excluded. The stepwise MLR was performed using the ancillary data of easting, northing, red, green, blue, EM31 and EM38 signal data. For each particle-size (i.e. clay, silt and sand) an individual model was developed from the ancillary data. The successful model was then used to predict the various particle-size fractions across each field.

Before the model could be applied, the EM31 and EM38 signal data and the red, green, blue values needed to be calibrated to the common 5m grid. The survey transects that the MESS followed to collect measurements of ECa were not of the same eastings and northings as the 5m grid. In order to make them the same the EM data collected from the survey transects was interpolated onto the 5m grid using ordinary kriging with the application Vesper. Similarly, when ERDAS Imagine extracted the red, green and blue values from the aerial photograph, values were obtained for each individual pixel in the digitised image. These values were also kriged onto the 5m grid using Vesper.

The regression model summary statistics and parameter estimates for the MLR models used for particle-size predictions of 'Midkin' Field 11 are given in Table 3.

Table 3 Mulitple Linear Regression (MLR) model summary statistics for estimation of particle size fractions for 'Midkin' Field 11.

1) Model Summary Statistics - Midkin Clay

Equation	$Clay = \beta_0 + \beta_1(northing) + \beta_2(red) + \beta_3(green) + \beta_4(EM38) + \beta_5(EM31) + \varepsilon$
RMSE	4.44
r^2	0.83

1) Parameter estimates - Midkin Clay

Coefficient	Parameter Estimate	Standard error	*t*-test	*p* >|*t*|
β_0	-218.05	147.06	-1.48	0.14
β_1	44.87	25.80	1.74	0.09
β_2	-0.19	0.04	-4.64	<0.0001
β_3	0.12	0.06	2.08	0.04
β_4	0.07	0.04	1.67	0.10
β_5	0.12	0.05	2.40	0.12

2) Model Summary Statistics - Midkin Silt

Equation	$Silt = \beta_0 + \beta_1(easting) + \beta_2(northing) + \beta_3(red) + \varepsilon$
RMSE	3.19
r^2	0.40

2) Parameter estimates - Midkin Silt

Coefficient	Parameter Estimate	Standard error	*t*-test	*p* >|*t*|
β_0	194.05	53.97	3.60	0.0006
β_1	17.74	8.36	2.12	0.038
β_2	-43.08	12.45	-3.46	0.0010
β_3	-0.14	0.02	-5.49	<0.0001

3) Model Summary Statistics - Midkin Sand

Equation	$Sand = \beta_0 + \beta_1(red) + \beta_2(green) + \beta_3(EM31) + \varepsilon$
RMSE	4.98
r^2	0.77

3) Parameter estimates - Midkin Sand

Coefficient	Parameter Estimate	Standard error	*t*-test	*p* >|*t*|
β_0	12.56	12.51	1.00	0.3194
β_1	0.27	0.05	5.09	<0.0001
β_2	-0.13	0.04	-3.47	0.0010
β_3	-0.20	0.03	-6.87	<0.0001

Table 4 Mulitple Linear Regression (MLR) model summary statistics for estimation of particle size fractions for 'Warianna' Field 4.

1) Model Summary Statistics - Warrianna Clay

Equation	$Clay = \beta_0 + \beta_1(easting) + \beta_2(green) + \beta_3(EM31) + \beta_4(EM38) + \varepsilon$
RMSE	4.02
r^2	0.75

1) Parameter estimates - Warrianna Clay

Coefficient	Parameter Estimate	Standard error	*t*-test	$p > \|t\|$
β_0	-156.13	172.09	-0.91	0.3707
β_1	64.57	54.98	1.17	0.2483
β_2	-0.28	0.13	-2.20	0.0346
β_3	-0.23	0.09	-2.62	0.0130
β_4	0.60	0.13	4.45	<0.0001

2) Model Summary Statistics - Warrianna Silt

Equation	$Silt = \beta_0 + \beta_1(easting) + \beta_2(northing) + \varepsilon$
RMSE	4.36
r^2	0.14

2) Parameter estimates - Warrianna Silt

Coefficient	Parameter Estimate	Standard error	*t*-test	$p > \|t\|$
β_0	-303.13	283.71	-1.07	0.2924
β_1	-85.12	53.12	-1.60	0.1178
β_2	70.25	32.13	2.19	0.0354

3) Model Summary Statistics - Warrianna Sand

Equation	$Sand = \beta_0 + \beta_1(green) + \beta_2(EM31) + \beta_3(EM38) + \varepsilon$
RMSE	3.37
r^2	0.77

3) Parameter estimates - Warrianna Sand

Coefficient	Parameter Estimate	Standard error	*t*-test	$p > \|t\|$
β_0	25.74	14.10	1.83	0.0765
β_1	0.21	0.10	2.08	0.0450
β_2	0.26	0.07	3.60	0.0010
β_3	-0.61	0.11	-5.45	<0.0001

3.4 Spatial Prediction of PSF

3.4.1 Spatial Distribution of Predicted Clay Content

Table 3 shows the MLR models derived from the ancillary information to predict the particle-size distribution of any point on the 5 m grid. Overall, the EM31 signal data had the best correlation with clay and sand content of 'Midkin' Field 11 with r2 values of 0.65 and 0.56 respectively. However, the clay and sand content of 'Warrianna' Field 4 had the best correlation with the EM38 signal data with r2 values of 0.83 and 0.81 respectively. It is generally accepted that clay content can be one of the main contributing factors to the response of the EM instrument, especially where salinity is not strongly present in the soil. The EM signal data can therefore be used to predict clay content of both fields.

The spatial prediction of the clay content of 'Midkin' and 'Warrianna' fields is shown in Figure 11a) and b). The percentage clay content is predicted for an average depth of 1.5 m for 'Midkin' and 2.1 m for 'Warrianna'. Both fields have predicted clay content of approximately similar range. For 'Midkin' Field 11 the range is 23-76% and for 'Warrianna' Field 4 the range is 25-74%. The mean clay content was 55% for 'Midkin' and 51% for 'Warrianna'.

Figure 11a) shows the predicted clay content of 'Midkin' Field 11 is highest in the north-eastern section of the field with values of over 65%, which texturally this as a heavy clay. The clay content remains relatively high (up to 60%) along the northern boundary and grades into lighter clays in the south-western part of the field where clay content ranges between 40-50%. The prior stream channels are particularly evident. The main channel can be seen quite clearly extending from the central southern end of the field, running almost parallel with the western boundary toward the northwest. The smaller, less obvious palaeochannel is located in the southwestern corner of the field. Levels of clay content within these palaeochannels is less than 40%.

Figure 11b) shows the predicted clay content is greatest in 'Warrianna' Field 4 along the northern and western sections of the field where clay content is 60 to >70%. The eastern and southeastern sections of the field have the lowest predicted clay content (i.e. <50%). Intermediate

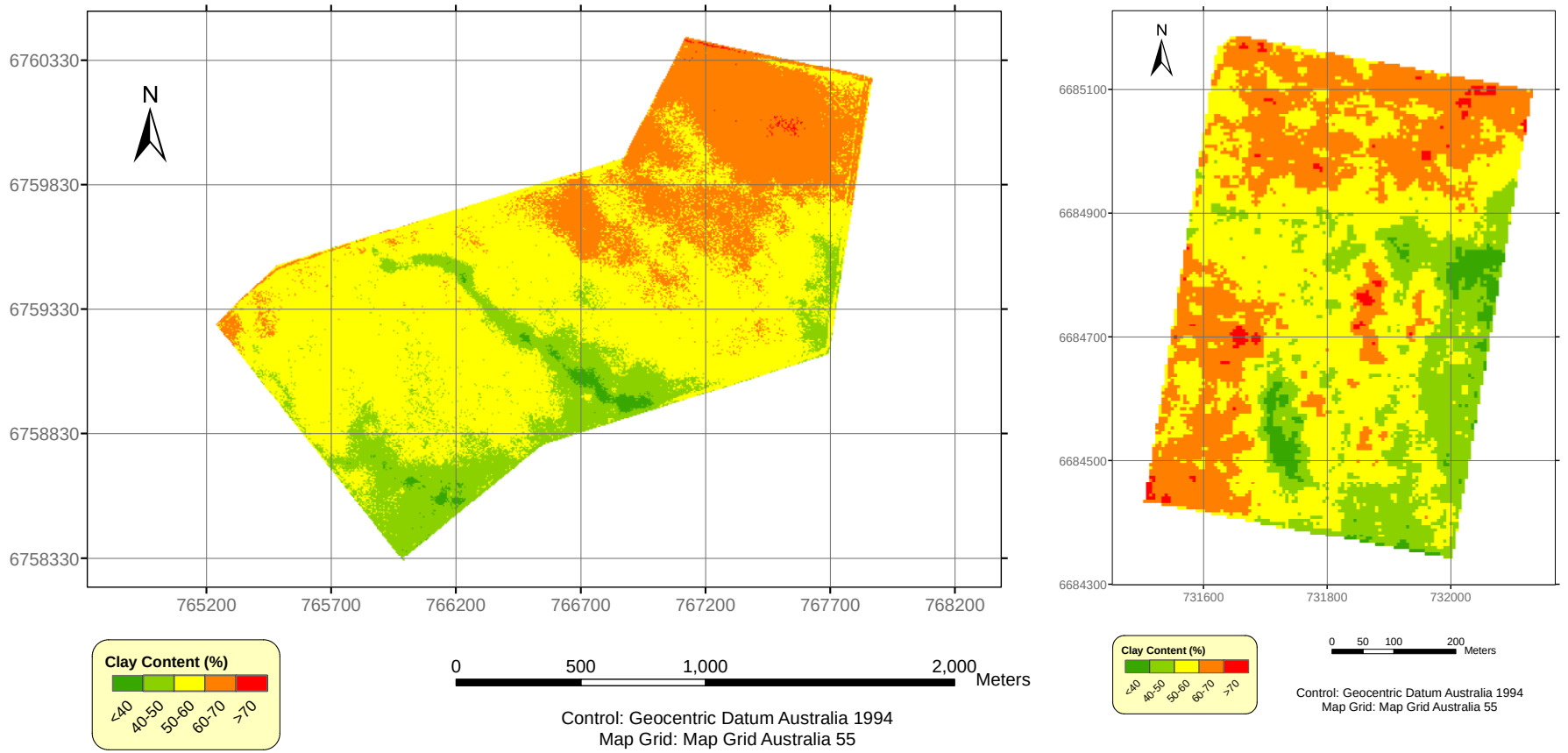

Figure 11 Spatial distribution of predicted clay content across a) 'Midkin' Field 11 and b) 'Warrianna' Field 4.

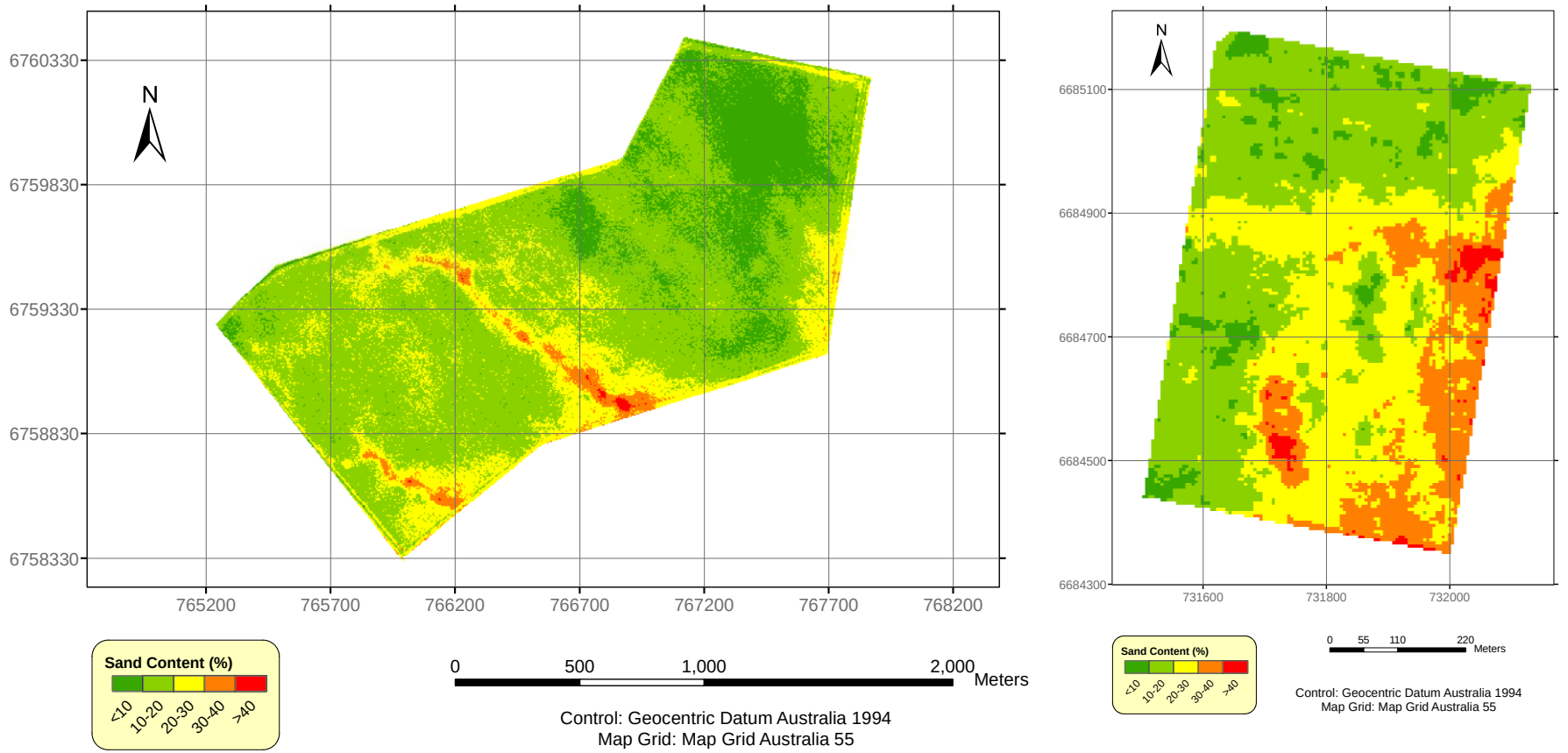

Figure 12 Spatial distribution of predicted sand content across a) 'Midkin' Field 11 and b) 'Warrianna' Field 4.

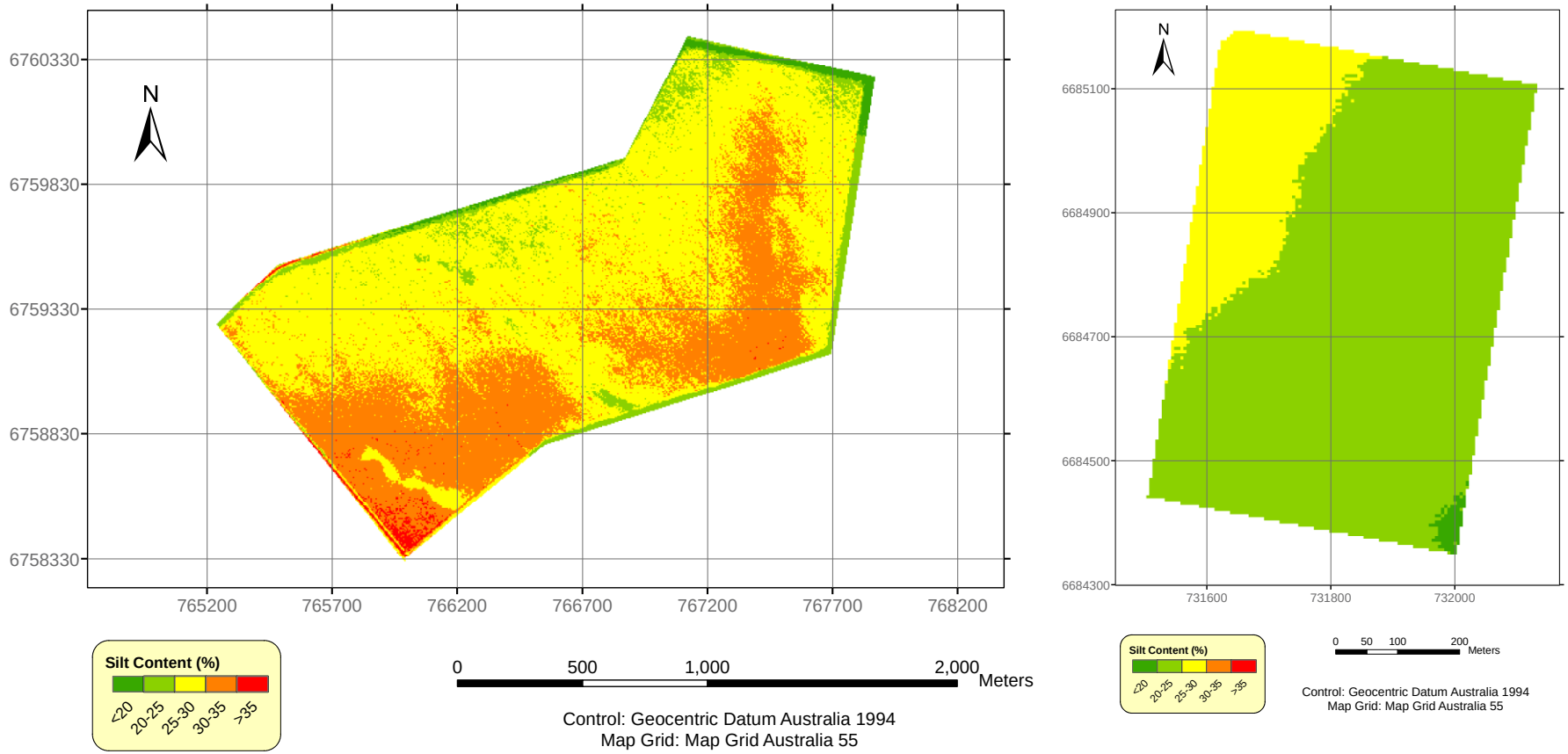

Figure 13 Spatial distribution of silt content across a) 'Midkin' Field 11 and b) 'Warrianna' Field 4.

levels of clay content occupy a contiguous area which covers the central part of the field. However, it is worth noting that an island of low clay content is evident in the central southern part of this field where EM signal data values are low and red and green reflectance values were intermediate.

3.4.2 Spatial Distribution of Predicted Sand Content

Figure 12a) shows the spatial distribution of predicted sand content of 'Midkin' Field 11. Unsurprisingly, predicted sand content is greatest within the palaeochannels (i.e. >40%). Conversely, sand content is lowest (i.e. <10%) in the northeastern section of Field 11 where clay content was greatest. Intermediate levels of sand content occur on the edges of the prior stream channels.

Figure 12b) shows the spatial distribution of predicted sand content across 'Warrianna' Field 4. Sand content is greatest (i.e. >30%) in the eastern section of the field and where the elliptical shape occurs in the southern section. This sandy lens is also visible in the aerial photograph of Field 4. These areas can be compared to the same location in Figure 11b) where predicted clay content is lowest (40-50%). Areas of the field where sand content is low (i.e. <20%) occur roughly in the northern and western sections of the field. These areas generally coincide with the same locations in Figure 11b) where clay content is more than 60%.

3.4.3 Spatial Distribution of Predicted Silt Content

Figure 13a) shows the spatial distribution of the predicted silt content of 'Midkin' Field 11. The areas of highest silt content (i.e. >30%) occur in the southern and southwestern parts of the field with exception to the locations of the prior stream channels. The prior stream channels can be identified by the areas mapped in yellow and green representing silt content of <30%. As mentioned previously, the soil texture here is sandier rather than siltier. In relation to Figure 12a) where silt is highest in the southwestern corner, it is worth noting that the clay content is lowest. Conversely, in the northeastern corner, where silt content is low, clay content is the highest in the field (i.e. >60%).

Figure 13b) shows the predicted silt content of 'Warrianna' Field 4. A suitable regression relation ship was not able to be developed from any of the known ancillary variables, hence the low r^2 value (i.e r^2=0.14). The model was able only to predict a very general trend based on the easting and northing predicting lowest silt content in the southeastern corner gradually increasing towards the northwestern corner. In light of the weak regression relationships, silt content was calculated by difference. As the MLR models for sand content and clay content had fairly high r^2 values of 0.77 and 0.75 respectively, it was considered appropriate to estimate the silt content of Field 4 by difference rather than by MLR.

3.5 Predicted Moisture Retention Curves From Neurotheta

3.5.1 Field Capacity

Field capacity represents the upper limit of the total plant available water content after saturation where the matric potential of water is -33 J/kg. Figure 14a) shows the spatial distribution of volumetric moisture held at field capacity (FC) of 'Midkin' Field 11. The area where the most water is held at field capacity is located in the northeastern corner of the field which also coincides with the locations of the highest measured EC_a for both EM31 and EM38 signal data as well as the highest predicted clay content of the field. The predicted field capacity of this area is >0.45 cm^3/cm^3 and is represented in dark purple. These are the heavy grey cracking clay (i.e. Vertosol) soil types.

The areas of the field with the lowest volumetric moisture (i.e. 0.3-0.4 cm^3/cm^3) at field capacity are represented in Figure 14a) in yellow and brown. It is obvious that these areas also spatially coincide with the locations of the prior stream channels and other sandier sections of the field. This is consistent with the fact that sandier or coarser textured soils hold the least amount of water and have the fastest rate of water movement. As soils become finer textured (i.e. higher clay content) the water holding capacity increases as clay particles are negatively charged and hold on to more water than sand particles. Loams and clay loams tend to have the highest available water capacity, however, the AWC of a clay soil is less. The rest of the field is characterised by mid-range field capacity of 0.4-0.45 cm^3/cm^3. It is interesting to note that the areas along the northern boundary where the higher clay content was predicted has a predicted moisture content at FC (i.e. 0.35-0.40 cm^3/cm^3) which is less than the lower clay content areas directly south-east of it. The moisture at FC here (represented in purple) is 0.40-.045 cm^3/cm^3.

Figure 14b) shows the spatial distribution of volumetric moisture held at field capacity of 'Warrianna' Field 4. Most of Field 4 has an estimated Field Capacity of 0.40-0.45 cm^3/cm^3. A comparison can be drawn between this figure and Figure 11b). The areas of lowest moisture at FC (i.e. 0.30-0.40 cm^3/cm^3) also coincide with the areas of lowest clay content and greatest sand

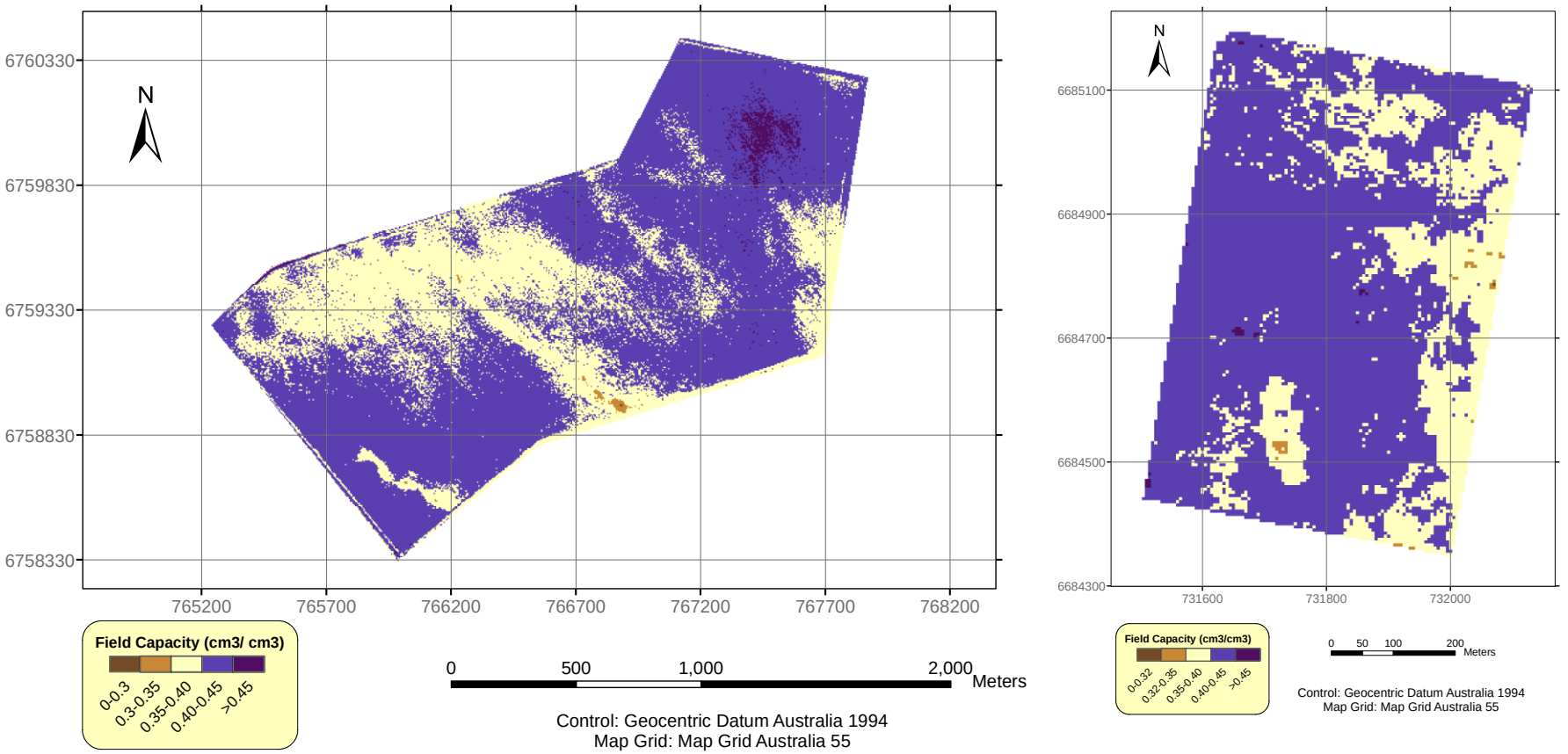

Figure 14 Spatial distribution of volumetric moisture at field capacity across a) 'Midkin' Field 11 and b) 'Warrianna' Field 4.

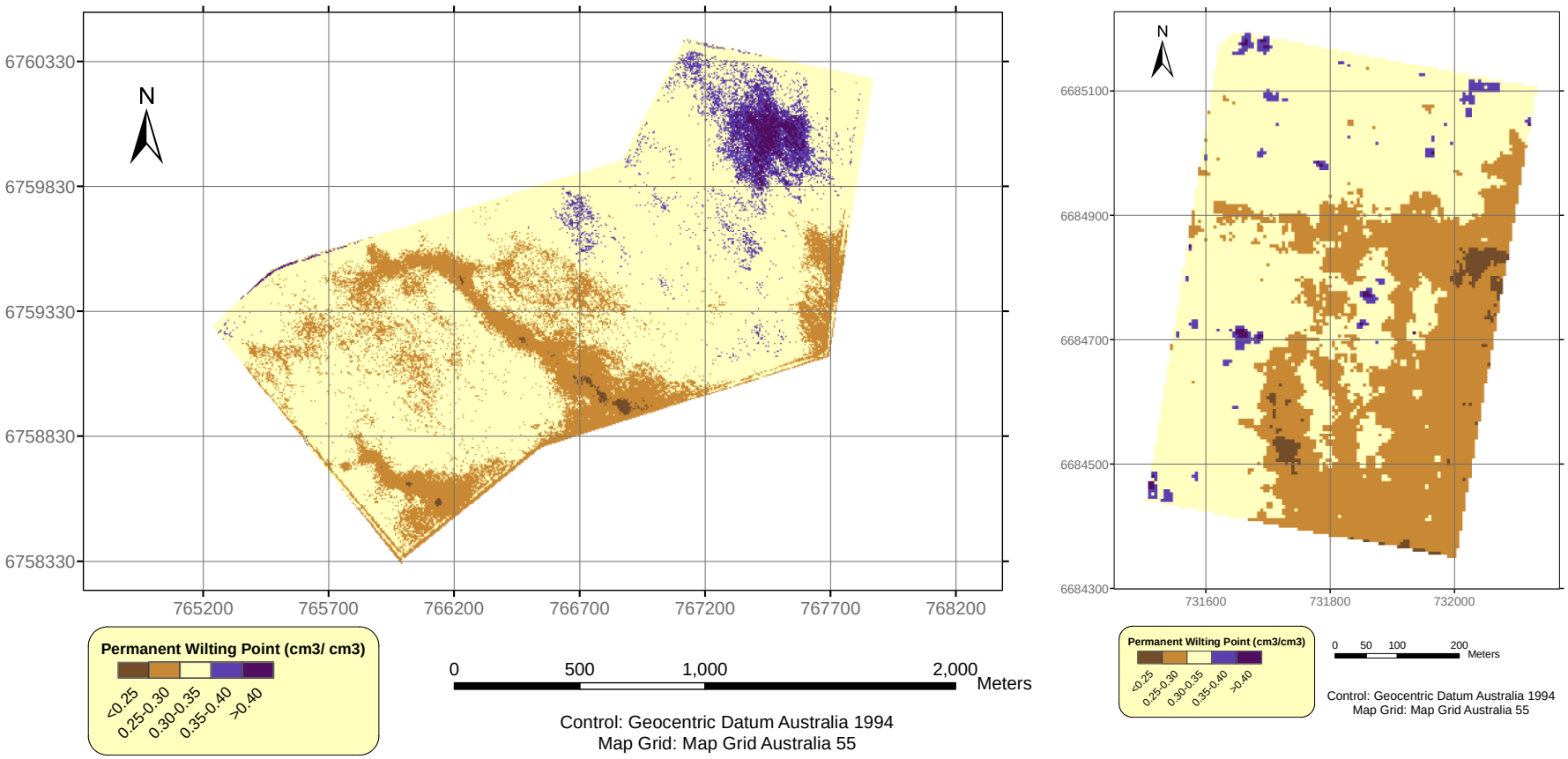

Figure 15 Spatial distribution of volumetric moisture at permanent wilting point across a) 'Midkin' Field 11 and b) 'Warrianna' Field 4.

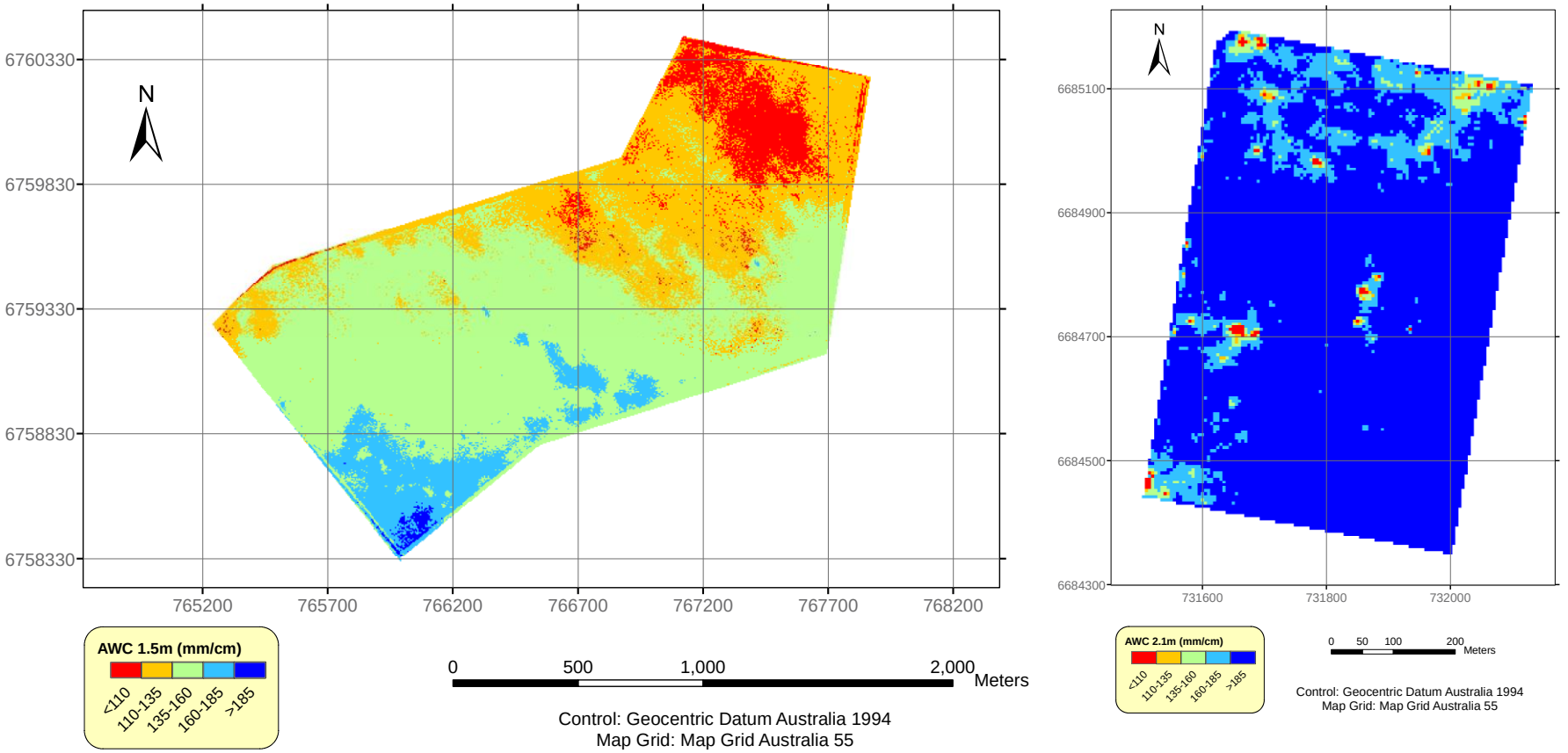

Figure 16 Spatial distribution of available water content across a) 'Midkin' Field 11 and b) 'Warrianna' Field 4.

content. These areas are mapped in cream in Figure 14b). The eastern and southern part of the field where this volumetric level of FC occurs coincides with greatest sand content. This is consistent with textured soil holding less water at FC than finer textured soils.

3.5.2 Permanent Wilting Point

The permanent wilting point (PWP) represents the lower limit of the total plant available water content where a plant wilts overnight and cannot regain its turgidity. The matric potential of the soil water is -1500 J/kg. Figure 15a) shows the spatial distribution of volumetric moisture available at permanent wilting point across 'Midkin' Field 11. Again, the prior stream channels can be discerned by the brown colour representing low volumetric moisture content of 0.2-0.3 cm^3/cm^3 typical of sandy textured soils. Whereas Figure 13a) was mostly dominated by two different amounts of FC, PWP occurs at mostly the same volumetric moisture content across the field (i.e. 0.30-0.35 cm^3/cm^3), except the palaeochannels and north-eastern corner of high clay content. Figure 14b) shows the spatial distribution of PWP across 'Warrianna' Field 4. Areas of lowest moisture at PWP (<0.25-0.30 cm^3/cm^3) are mapped in brown and occur generally in the southeast.

3.5.3 Available Water Content

The sand, silt and clay fractions were predicted onto the 5 m common grid and these values were used as pedotransfer functions in Neurotheta to predict the MRC for all points on the 5 m grid. Figure 16a) shows the predicted spatial distribution of the available water content of 'Midkin' Field 11. The areas of high AWC (i.e. >160 mm/cm) are mapped in blue and the areas of low AWC (i.e. <135 mm/cm) are mapped in orange and red. The model predicted that the highest AWC occurs in the southwestern corner of the field where silt content is highest. The soil with the lowest AWC occurs in the northeast part of the field where predicted clay content is at its highest and predicted silt content moderate to high. The rest of the field has a predicted AWC of 135-160 mm/cm. Figure 16b) shows the spatial distribution of predicted AWC for 'Warrianna' Field 4. Most of the field has a predicted AWC of more than 185 mm/cm. The areas of highest AWC (i.e. >185 mm/cm) coincide with Figure 11b) where predicted clay content is <40-60%.

4. CONCLUSIONS

The aims of this study were to predict the available soil moisture content of various soil types in two irrigated cotton growing field in the lower Namoi and Gwydir valleys. This was achieved by first predicting the soil texture properties (i.e. clay, silt and sand percentages of the fine earth fraction) across each field using Multiple Linear Regression (MLR) equations between clay, silt and sand and information collected using electromagnetic (EM) induction instruments (i.e. EM38 and EM31) and red, green and blue reflectance bands obtained from a digitised air photo of these fields. This information was inputted into Neurotheta to estimate various soil water properties such as field capacity (FC), permanent wilting point (PWP) and determination of available water content (AWC). The results are equivocal. In the case of the "Midkin" field the results appear to be consistent with the farmers experiences and knowledge of soil water properties of this field. In the "Warrianna" field it appears the silt content was not be estimated as well and hence it led to overestimated values in FC, PWP and hence AWC.

The research however does point to future work that may be followed up in any further investigation. In the first instance the soil water estimates of FC, PWP and AWC should be validated with actual measurements taken to determine these parameters of the samples available. The pressure plate or filter paper method would appropriate. In addition, and once validated the results should be used in water balance models to compare and contrast the water use efficiency of soil water storage using the current irrigation method and various alternative approaches (i.e. travelling sprinkler irrigations) in these fields. In addition, and to resolve differences in mineralogy in the clay component, which has a significant effect on a soil type's ability to hold water, could also be conducted. This could be added to a database where the original data collected in this field along with data that can be collected using more district and regional sampling schemes. This type of project is relevant to the CRC's strategic goals as set out in the executive summary. Specifically to "Improve water use efficiency" and "Increased on-farm water use efficiency across the industry." Namoi and Gwydir Rivers.

5. ACKNOWLEDGMENTS

In the first instance I would like to thank the Cotton Communities and Catchment Cooperative Research Centre for the Summer Scholarship (2006/2007). I have really enjoyed working in a research environment and in particular being able to apply some of the skills and theoretical knowledge I have gained thus far in my undergraduate studies at the University of New South Wales, in a practical and applied research project. In this regard I would also like to thank and acknowledge Dr John Triantafilis (School of Biological Earth and Environmental Sciences) for encouraging me to undertake this program of research and for assisting in the development of an interesting and challenging research topic in the area of soil and water inter-relationships and the application of ancillary data with soil information to develop environmental correlations and subsequently digital soil maps.

During the course of this project I interacted on a daily basis with various research students and staff working in the area of soil and water research in the School of Biological Earth and Environmental Sciences at the University of New South Wales. I really enjoyed the scientific support and camaraderie of Mr Sam Buchanan (PhD student) and Dr Thomas Bishop. Specifically Sam was of great technical help and guidance on all things Geographic Information Systems (GIS). He also helped guide me through the digitisation, rectifying and extraction of red, green and blue data from a digital air photo using the Imagine software package. I would also acknowledge Dr Thomas Bishop (Research Fellow) who assisted greatly in the development of my understanding in forward selection modelling and step-wise linear regression analysis in developing environmental correlations and multiple linear regression relationships between the various ancillary data sources and the soil particle size fractions.

6. REFERENCES

Bishop, T.F.A. and McBratney, A.B., (2001), 'A comparison of prediction methods for the creation of field-extent soil property maps', *Geoderma*, Vol. 103, pp. 149-160.

Brevik, E.C. and Fenton, T.E., (2002), 'Influence of soil water content, clay, temperature, and carbonate minerals on electrical conductivity readings taken with an EM-38', *Soil Survey Horizons*, Vol. 43, pp. 9-13.

Coventry, R.J. and Fett, D.E.R., (1979), 'A pipette and sieve method of particle size analysis and some observations on its efficacy', *CSIRO Div. of Soils, Div. Rep. No. 38*, CSIRO, Australia.

De Jong, E., Ballantyne, A.K., Cameron, D.R., Read, D.W.L., (1979), 'Measurement of apparent electrical conductivity of soils by n electromagnetic induction probe to aid salinity surveys', *Soil Science Society of America Journal*, Vol. 43, pp. 810-812.

Foth, H..D., (1990), 'Fundamentals of Soil Science', John Wiley and Sons.

Lesch, S.M., Strauss, D.J. and Rhoades, J.D., (1995), 'Spatial prediction of soil salinity using electromagnetic induction techniques 1. Statistical prediction models: a comparison of multiple linear regression and cokriging', *Water Resources Research*, Vol. 31, No. 2, pp. 373-386.

Minasny, B. and McBratney, A.B., (2002), 'The neuro-m method for fitting neural network parametric pedotransfer functions', *Soil Science Society of America Journal*, Vol. 66, pp. 352-361.

Minasny, B., McBratney, A.B., and Whelan, B.M., 2005. VESPER version 1.62. Australian Centre for Precision Agriculture, McMillan Building A05, The University of Sydney, NSW 2006. (http://www.usyd.edu.au/su/agric/acpa).

Stannard, M.E. and Kelly, I.D., (1968), 'Irrigation potential of the lower Gwydir valley', Water Conservation and Irrigation Commission, New South Wales, Australia.

Sudduth, K.A., Kitchen, N.R., Wiebold, W.J., Batchelor, W.D., Bollero, G.A., Bullock, D.G., Clay, D.E., Palm, H.L., Pierce, F.J., Schuler, R.T. and Thelen, K.D., (2005), 'Relating apparent electrical conductivity to soil properties across the north-central USA', *Computers and Electronics in Agriculture*, Vol. 46, pp. 263-283.

Triantafilis, J. and Lesch, S.M., (2005), 'Mapping clay content variation using electromagnetic induction techniques', *Computers and Electronics in Agriculture*, Vol. 46, pp. 203-237

Triantafilis, J. Ahmed, M.F. and Odeh, I.O.A., (2002), 'Application of a mobile electromagnetic sensing system (MESS) to assess cause and management of soil salinization in an irrigated cotton-growing field', *Soil Use Management*, Vol. 18, pp. 330–339.

Triantafilis, J. Huckel, A.I., Odeh, I.O.A., (2001), 'Comparison of statistical methods for estimating field-scale clay content using different combinations of ancillary variables', *Soil Science*, Vol. 166, No. 6, pp 415-427.

Tucker, B.M. (1974), 'Laboratory procedure for cation exchange measurements in soils', *CSIRO Div. of Soils, Tech. Paper No. 23*, CSIRO, Australia.

Varvel, G.E., Schlemmer, M.R., Schepers, J.S., (1999), 'Relationship between spectral data from an aerial image and soil organic matter and phosphorus levels', *Precision Agriculture*, Vol. 1, No. 3, pp. 291-300.

Williams, B.G. and Hoey, D., (1987), 'The use of electromagnetic induction to detect the spatial variability of the salt and clay contents of soils', *Australian Journal of Soil Research*, Vol. 25, pp. 21-27.